Comparison of Experimentally-determined and Model-estimated Attachment Efficiency for Predicting Nanoparticle Aggregation

by
Jasmin Joy Kennard

A THESIS

submitted to

Oregon State University

Honors College

in partial fulfillment of
the requirements for the
degree of

Honors Baccalaureate of Science in Chemical Engineering
(Honors Scholar)

Presented June 5, 2018
Commencement June 2018

AN ABSTRACT OF THE THESIS OF

Jasmin Joy Kennard for the degree of Honors Baccalaureate of Science in Chemical Engineering presented on June 5, 2018. Title: Comparison of Experimentally-determined and Model-estimated Attachment Efficiency for Predicting Nanoparticle Aggregation.

Abstract approved:_____
Jeffrey A. Nason

The widespread use of engineered nanoparticles (ENPs) in industrial applications and consumer products makes their release to the environment inevitable. Understanding the aggregation behavior of ENPs is crucial to understanding their fate, transport and toxicology in aquatic systems. This study investigated the comparability of experimentally-determined and model-estimated attachment efficiencies for hematite nanoparticles. Aggregation behavior of hematite was investigated in monovalent KCl solutions and polyvalent synthetic freshwater solutions via time-resolved dynamic light scattering (TR-DLS) and nanoparticle tracking analysis (NTA). Experimental findings show that the critical coagulation concentration for KCl with 25 mg L^{-1} hematite colloids is approximately 33 mM. Rates of aggregation in the synthetic freshwater were significantly faster than in an equivalent ionic strength of KCl, likely due to the influence of pH on the surface charge of hematite. The model-estimated attachment efficiencies at 5 minutes had a strong linear correlation with measured initial aggregation rate, indicating qualitative agreement between the measured and modeled behavior. However, at longer time intervals attachment efficiency varied, indicating that the model was not accounting for all processes. Lastly, a reduced size 3 ODE test system was found to have a stiffness ratio of at least 10^7 for all non-zero concentration combinations of N_1, N_2, and N_3, indicating that the model may not be operating within the region of absolute stability for Heun's method.

Key Words: Nanoparticles, Colloid, Aggregation, Hematite, Wastewater

Corresponding e-mail address: kennard.jasmin@gmail.com

©Copyright by Jasmin Joy Kennard
June 5, 2018
All Rights Reserved

Comparison of Experimentally-determined and Model-estimated Attachment Efficiency for Predicting Nanoparticle Aggregation

by
Jasmin Joy Kennard

A THESIS

submitted to

Oregon State University

Honors College

in partial fulfillment of
the requirements for the
degree of

Honors Baccalaureate of Science in Chemical Engineering
(Honors Scholar)

Presented June 5, 2018
Commencement June 2018

Honors Baccalaureate of Science in Chemical Engineering project of Jasmin Joy Kennard presented on June 5, 2018.

APPROVED:

_____

Jeffrey A. Nason, Mentor, representing Environmental Engineering

_____

Malgorzata Peszynska, Committee Member, representing Mathematics

_____

Mark Surette, Committee Member, representing Environmental Engineering

_____

Toni Doolen, Dean, Oregon State University Honors College

I understand that my project will become part of the permanent collection of Oregon State University, Honors College. My signature below authorizes release of my project to any reader upon request.

_____

Jasmin Joy Kennard, Author

Table of Contents

1 Introduction 1
1.1 Motivation 1
1.2 Hypothesis and Objectives 1
1.3 Approach 2
2 Background 3
2.1 Colloids and Nanoparticles 3
2.2 Environmental Impact of Nanomaterials 3
2.3 Particle Interaction Theory 4
2.4 Effect of Ionic Strength on Stability 7
2.5 Quantifying Aggregation 9
2.6 Existing Mathematical Model 9
3 Materials and Methods 11
3.1 Colloids and Nanomaterials 11
3.1.1 Hematite Colloids 11
3.2 Suspending Mediums 11
3.2.1 Potassium Chloride Solution 11
3.2.2 EPA Synthetic Freshwater 11
3.3 Time-Resolved Dynamic Light Scattering 11
3.1.1 Sample Preparation 11
3.1.2 Initial Rate of Aggregation Calculation 12
3.1.3 Calculation of Attachment Efficiency (α) and Critical Coagulation Concentration 13
3.2 Nanoparticle Tracking Analysis 13
3.2.1 Sample Preparation 14
3.2.2 Mass Balance Calculations 14
3.3 NTA Comparison to Model 15
4 Results 16
4.1 Time-Resolved Dynamic Light Scattering. 16
4.2 Nanoparticle Tracking Analysis. 21
4.3 Experimental and Modelling Comparison 24
4.4 Modelling Considerations 30

4.4.1 Investigations of System Stiffness 30
5. Conclusion 35
6. References 37
Appendices 39
Appendix A1. Initial Rates of Aggregation for Hematite in KCl 39
Appendix A2. KCl and $CaCl_2$ CCC data for 10 mg L^{-1} Hematite 40
Appendix A3. Summary of Model Inputs 41

List of Figures

Figure 1. Comparison of several trajectories in the rectilinear (left) and curvilinear (right) model, where the shaded region represents the critical separation distance for collision.[3] 6

Figure 2. Energy of interaction for particles approaching one another in (a) the reaction-limited regime, (b) at the CCC, and (c) in the diffusion-limited regime. The attractive forces are V_a, the repulsive forces are V_r and the total energy of interaction is V_t.[9] 8

Figure 3. Calculation of the initial aggregation rate from TR-DLS measurements. Solid circles indicate data used to calculate the slope. Results shown are for synthesized hematite colloids in 150 mM KCl. 12

Figure 4. Intensity-weighted hydrodynamic diameter of hematite colloids in various concentrations of potassium chloride. 17

Figure 5. Attachment efficiencies for hematite colloids as a function of KCl concentration. The CCC calculated from the data is 33 mM KCl. 18

Figure 6. TR-DLS profiles of intensity-weighted D_h for 25 mg L^{-1} synthesized hematite during aggregation in various concentrations of EPA test water. 19

Figure 7. Number-weighted particle size distribution of hematite colloids in moderately hard EPA test water, measured using Nanoparticle Tracking Analysis. 21

Figure 8. Comparison of the reported concentration of the various time measurements for hematite colloids in EPA test water. The DDI experiment average reports all samples prepared with DDI and KCl. 23

Figure 9. Particle size distributions of initial model input with time resolved particle size distribution outputs from the model. 24

Figure 10. Comparison of model-estimated attachment efficiency with experimental initial aggregation rate. 25

Figure 11. Comparison of experimental and modelled particle size distribution using $\alpha emp = 0.45$ for moderately hard synthetic freshwater at 20 minutes. 26

Figure 12. Comparisons of experimental results at 30 minutes with the model prediction from 10 to 30 minutes, using the attachment efficiency estimated from 0 to 10 minutes for (a) very soft water, (b) soft water, and (c) moderately hard water. 27

Figure 13. Model-estimated attachment efficiency based on time interval of comparison. .. 28

Figure 14. Screenshots from NTA of hematite colloids in 68 mM KCl: at (a) $t = 0$ min, (b) $t = 15$ min, and (c) $t = 30$ min. 29

Figure 15. Stiffness ratios of the system at constant N_3 concentrations of N_3 = 0, 10 and 20 mg L^{-1} with N_1 and N_2 concentrations varying between 0 mg L^{-1} and 20 mg L^{-1}..... 33

Figure 16. Initial rates of aggregation calculated using the time elapsed between the initial measurement and when the hydrodynamic diameter reached 1.3($D_{h,0}$). The horizontal line represents the average initial rate of aggregation for the trials from 0.050 M to 0.150 M KCl. 39

ACKNOWLEDGEMENTS

I would like to thank my advisor Dr. Jeff Nason for all his support and guidance during the last 4 years. When I started working in his lab, I never imagined what an impact it would have on my college experience and career aspirations. I would also like to thank Dr. Malgorzata Peszynska for sharing her wealth of knowledge to further my research goals and for being a member of my thesis committee. Thank you to Mark Surette for being on my thesis committee, and for his help with the flocculation model. I would also like to thank Dan Pike for all his help when I first started in the lab. Thank you to all the Nason lab members who have made the lab not only a place of learning but also a place of friendship. Thank you to Bryan Harper and Dr. Stacey Harper for the use of their NanoSight instrument, the results from which provide the basis of this thesis. Thank you, Pete and Rosalie Johnson, for providing the funding that made this opportunity possible for me and many other students. Finally, I would like to thank my friends and family for supporting and encouraging me in this endeavor and all others.

1 Introduction

1.1 Motivation

In past decades, engineered nanoparticles (ENPs) have been increasingly utilized in a wide variety of industries, from industrial production to food technology, and nanoscience now represents a multibillion dollar industry. Due to their high-volume production and widespread use, ENPs produced in factories and laboratories to be used in common consumer products like cosmetics and sunscreens are unavoidably introduced into the environment. The manufacturing and use of ENPs has outpaced the research on potential consequences to human health and the environment of long-term exposure to environmental ENPs, whose disposition and bioavailability is largely determined by their distribution, fate and physicochemical properties.

Recent literature expresses the understanding that nanomaterials undergo extensive physicochemical transformations in the environment and that analyses of environmental risk should focus on the transformed species.[1] Likely transformations include homoaggregation, heteroaggregation, and adsorption of macromolecules, such as natural organic matter (NOM). To better assess the toxicological risks of ENPs in the environment, the scientific community must understand how these particles undergo transformations in the environment.

Aggregation is the formation of clusters of colloidal particles in a colloidal suspension. During this process, particles dispersed in the liquid phase stick to each other and spontaneously form irregular particle clusters, called aggregates. Homoaggregation refers specifically to aggregation between particles of the same species, while heteroaggregation refers to aggregation between particles of different species. Aggregation occurs when the particles have been destabilized (altering the forces between particles to be less repulsive), either by a coagulant, adsorption, or due to changes in aquatic chemistry, such as in ionic strength or pH. The extent to which ENPs aggregate influences the rate of ENP gravitational settling and determines whether particles accumulate in sediments and soils or stay suspended in the water column.

This study intends to compare the changes in the particle size distribution of nanoparticles and colloids as measured by Nanoparticle Tracking Analysis with changes predicted by a mathematical model for particle aggregation. Hematite was chosen as a model colloid due to the considerable interest in noble metal nanoparticles in various fields and its increased use.[2] Its wide applications and its unique size-dependent properties make hematite an appropriate ENP to study. It is also representative of naturally occurring colloids and has been the subject of substantial research.

1.2 Hypothesis and Objectives

The goal of this study was to investigate the accuracy of an existing mathematical model of particle aggregation developed by Nason[3] via the comparison with particles size distributions measured via Nanoparticle Tracking Analysis. It is hypothesized that the experimentally-measured and model-estimated attachment efficiencies will be similar, indicating that the model

accurately predicts the aggregation behavior of the model colloids in various solution chemistries. Discrepancies between the model and the experimental results will identify areas for continued work. Specific objectives of the research are as follows:

1. Experimentally measure the aggregation behavior of model colloids in synthetic aquatic media.
    a. Compare results from two methods of experimental aggregation measurement: time-resolved dynamic light scattering and nanoparticle tracking analysis.
2. Mathematically model colloid aggregation to predict the evolving size distribution and compare with experimental results.
3. Evaluate the suitability of the current numerical scheme and time step used in the mathematical model.

1.3 Approach

Each objective was achieved using model colloids synthesized by members of the Nason lab, or via the use of the model developed by Nason.[3] Experimental trials were compared to the modelled particle size distributions to determine the corresponding attachment efficiencies of each system. The approach used to accomplish each specific objective is outlined below.

1. Time-resolved dynamic light scattering was used to determine the change in average hydrodynamic diameter from which the experimental attachment efficiencies were calculated. Nanoparticle Tracking Analysis was used to determine the particle size distributions of the samples over time.
2. The initial size distributions found in objective 1 were input into the Nason model, and the model output was compared to the data collected via NTA to determine the model-predicted attachment efficiencies.
3. Evaluation of system stiffness occurred via the linearization of a test system and subsequent eigenanalysis.

The remainder of this thesis is organized as follows. Chapter 2 contains a literature review detailing previous work on the fate and transport of colloids and nanoparticles in the environment. Chapter 3 describes the model colloids, solutions, methods and analytical techniques used. Chapter 4 presents and discusses the results obtained. Chapter 5 concludes and suggests direction for future work. Chapter 6 contains the references cited in this thesis.

2 Background

2.1 Colloids and Nanoparticles

Colloids are an intermediate between solutions (homogeneous mixtures whose component elements are small enough that thermal motions overcome the effects of gravity) and suspensions (heterogeneous mixtures in which the suspended particles are sufficiently large to settle out of solution). Colloidal dispersions appear to be homogenous, and the colloidal particles are small enough to experience Brownian motion (the erratic random movement of microscopic particles in a fluid from the continuous bombardment by molecules of the surrounding medium), but the particles can settle out of solution when destabilized. Colloidal systems generally include particles with one or more dimensions in the range of approximately 1nm up to 1μm. Nanoparticles are a subset of colloids. An engineered nanoparticle is classified as any anthropogenic particle with one or more dimensions between 1 and 100 nm (1 nm=10^{-9} m) in length. Nanomaterials and colloids are of great interest because, unlike bulk materials, which have constant physical properties at any size, they can possess unexpected size-dependent characteristics, often due to their extremely high surface area to volume ratios. This means that colloids and nanoparticles of the same atomic species could possess vastly different physical properties at different sizes.

2.2 Environmental Impact of Nanomaterials

Due to the high surface-to-volume ratios of nanomaterials, many nanomaterials are used in a wide variety of novel applications. Some, like carbon nanotubes, have unique electrical properties on the nano-scale and are used in medicines, for energy storage and in the production of semiconductors.[4] Nanomaterials are being widely used, with a recent study reporting that up to 10,000 tons of titanium dioxide nanomaterials are produced annually for use in cosmetics, sunscreens, pigments and as additives in food.[5] Nanomaterials can be of toxic concern in the environment.[1] Due to their high reactivity, nanoparticles in the environment are transformed from their original, synthesized state by a myriad of processes, including aggregation and reactions with natural macromolecules.[6] The size of nanoparticles is an important determinant of reactivity, transport, and toxicity. Nanoparticles tend to be present in the environment as aggregates, and light scattering techniques are often employed to study nanoparticle stability in solution.[6] The study of nanoparticles in the environment is made difficult by the variety of nanomaterial composition, shape, size and coatings, and further complicated by the range of solution chemistries, types and quantities of natural organic matter and presence of other nanomaterials in the environment, which makes nanomaterial behavior in these complex systems difficult to predict.[1] In addition, ENPs are often composed of elements that are already abundant in the environment, and modelling efforts suggest that they are present only at low environmental concentrations, making them difficult to detect and hard to distinguish from natural colloids and other contaminants. Because of the difficulty of measuring nanoparticles in the environment, a substantial amount of research has focused on the creation of models to predict nanoparticle fate and transport.

2.3 Particle Interaction Theory

Particle interaction theory has been researched for over a century. These studies have primarily focused on the interaction of colloids significantly larger than nanoscale. There have been limited attempts to measure and model aggregation of particles in the nanoscale range. This study aims to bridge the gap in understanding. The aggregation behavior of colloids and nanoparticles in aquatic systems is a product of particle-particle interactions, which are influenced by many factors. For particles in aqueous systems, the characteristic transport length is typically two or more orders of magnitude larger than the largest particles in the system.[7] There are two regions of transport that must be considered: rectilinear transport, which considers only long-range forces described by the collision frequency function, and curvilinear transport, which uses the collision frequency function in conjunction with a corrective factor accounting for short-range forces. Long-range transport can occur via three mechanisms: Brownian motion, due to kinetic energy at a given temperature; differential sedimentation, due to particle density and gravitational forces; and fluid shear, due to non-constant velocity profiles of fluid flow. In the rectilinear model, the critical separation distance between two interacting particles' centers of mass is given by the sum of their radii, because any smaller distance will result in a collision, see Figure 1.

In discrete form, the Smoluchowski equation describes the rate of particle aggregation based on number concentration (N) and collision frequency functions (β) for each of the long-range transport mechanisms listed previously.[8]

$$^{Aggregation}r_k = \frac{dN_k}{dt} = \frac{1}{2}\alpha_{emp} \sum_{\substack{all\ i\ and\ j \\ such\ that \\ V_i+V_j \\ =V_k}} \gamma_{ij} N_i N_j - \alpha_{emp} N_k \sum_{all\ i} \gamma_{ij} N_i$$

$$\text{where: } \gamma_{ij} = {}^{Br}\beta_{ij} + {}^{Sh}\beta_{ij} + {}^{DS}\beta_{ij}$$

where i and j are subscripts denoting particle size classes, N_i is the number concentration of particles of size i, and β_{ij} is the collision frequency function describing collisions between particle sizes i and j. The first term on the right-hand side describes the gain of particles of size k via the aggregation of particle sizes whose combined volumes sums to the volume of particle size k. The second term is a loss term which describes the aggregation of particles of size k with all other particle sizes.

The collision frequency functions for the three long-range mechanisms are written as follows, where d_i is the diameter of particle i and d_j is the diameter of particle j.

For Brownian motion,

$$^{Br}\beta_{ij} = \frac{2kT}{3\mu}\left(\frac{1}{d_i} + \frac{1}{d_j}\right)(d_i + d_j)$$

For fluid shear,

$$^{Sh}\beta_{ij} = \frac{G}{6}(d_i + d_j)^3$$

For differential sedimentation,

$$^{DS}\beta_{ij} = \frac{\pi g}{72\mu}(\rho_{particle} - \rho_{liquid})(d_i + d_j)^3|d_i - d_j|$$

where, k is the Boltzmann constant, T is absolute temperature, μ is the fluid viscosity, G is the average velocity gradient, g is the gravitational constant, and $\rho_{particle}$ and ρ_{liquid} are the bulk densities of the particle and the liquid, respectively. This model relies on several key assumptions. It is assumed that all collisions result in aggregation, that fluid motion is governed by laminar shear, that aggregate breakup is negligible, that collisions occur between only two particles, and that particles are hard spheres which, after aggregation, form another hard sphere where volume is conserved, and aggregate porosity is not considered.[3]

The rectilinear model accounts for the short-range forces using the empirical alpha parameter (α_{emp}), which represents the attachment efficiency, a parameter between 0 and 1 indicating the number of collisions which result in attachment.

The curvilinear model considers several additional short-range forces that are not relevant at great distance but become relevant at close range. First, that water must move out of the way for particles to collide. These hydrodynamic interactions influence particle movement and tend to prevent particle collisions. Second, van der Waals forces become significant at close range and act to promote particle collisions. Third, charged particles develop diffuse layers of counter-ions which tend to promote collisions between oppositely charged particles and prevent particle collisions between oppositely charged particles. These forces combine to reduce the critical separation distance with respect to the rectilinear model. For these reasons, the curvilinear model predicts a lower number of collisions than the rectilinear model. A diagram showing some potential particle trajectories is shown in Figure 1.

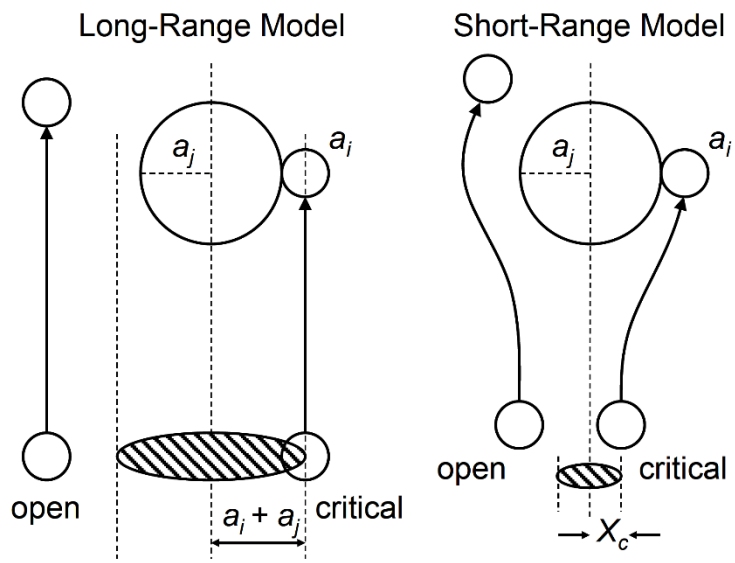

Figure 1. Comparison of several trajectories in the rectilinear (left) and curvilinear (right) model, where the shaded region represents the critical separation distance for collision.[3]

Derjaguin-Landau-Verwey-Overbeek (DLVO) theory describes the interactions between colloidal particles in terms of the net interaction energy between particles. The theory proposes that particle aggregation is determined by two forces, van der Waals attractive forces and electrostatic repulsive forces.

Van der Waals forces are weak, short-range attractive forces between uncharged molecules arising from temporary dipole created by the random distribution of electrons in the particles.[7] Van der Waals forces are only significant at very close range, so it only affects particle interactions if there is little electrostatic hinderance to the particles approach relative to their kinetic energy. The van der Waals attractive energy for two particles is a function of both the particle sizes and the intensive Hamaker constant.

The electrostatic double layer forces derive from the surface charge of a particle. A particle's surface charge creates an electrical potential field that is strongest near the particle surface and weakens as the distance from the surface increases. Due to the electrical potential, a thin layer of counter-ions is attached to the particle surface and the volume surrounding the particle develops a relative surplus of free counter-ions and a relative scarcity of free co-ions. The thin layer of bound counter-ions is called the stern layer and the high concentration of counterions surrounding that layer is called the diffuse layer. There also exists a shear layer within the diffuse layer and whose boundary indicates the distance at which a shear plane develops separating the ions which move with the particle from those in the bulk solution.

The energy of interaction for two identical spherical particles can be plotted as a function of the distance between the two interacting particles. When particles of opposite charge approach one another, the electric potential causes an electrostatic attractive force because they are also of

opposite charge. When particles of the same charge approach one another, the electrical potential fields will begin to interact, causing a repulsive force due to their like charge. If the repulsion experienced between the particles due to the electrical potential fields is larger than the attractive van der Waals forces, the particles will not aggregate.

For the curvilinear model, the Smoluchowski equation is modified to include a collision efficiency correction factor (α_{ij}) to more accurately predict the number of collisions based on the smaller critical separation distance. This factor accounts for van der Waals attraction and hydrodynamic effects but does not account for double layer interactions because double layer interactions are strongly related to solution and particle characteristics. The inclusion of the collision efficiency correction factor for each long-range transport mechanism is shown below.

$$\gamma_{ij} = {}^{Br}\alpha_{ij}\,{}^{Br}\beta_{ij} + {}^{Sh}\alpha_{ij}\,{}^{Sh}\beta_{ij} + {}^{DS}\alpha_{ij}\,{}^{DS}\beta_{ij}$$

For differential sedimentation and fluid shear, the collision efficiency correction factor takes the same form. The transport mechanisms are conceptually similar because the particle trajectories of both are parallel and linear. However, the critical separation distance is different for the two mechanisms.

$${}^{Sh,DS}\alpha_{ij} = \frac{X_C^2}{\left(d_i + d_j\right)^2}$$

For Brownian motion the collision efficiency factor takes the following form,

$${}^{Br}\alpha_{ij} = a + b\lambda + c\lambda^2 + d\lambda^3$$

where a, b, c and d are experimentally determined constant coefficients and λ is the size ratio ($0 < \lambda \leq 1$) between the particles.[8]

2.4 Effect of Ionic Strength on Stability

As mentioned previously, DLVO theory describes aggregation as a product of the net interaction energy of particles approaching one another. The total energy of interaction is the sum of the repulsive and attractive forces. One method to destabilize charged particle suspensions to promote aggregation is to increase the ionic strength of the solution. The ionic strength of a solution is a measure of the free ions in solution and is calculated using the equation below.

$$I = \frac{1}{2}\sum_{i=1}^{n} c_i {z_i}^2$$

where I is the ionic strength, c_i is the molar concentration of ion i, and z_i is the ionic charge of ion i. The summation is taken over all the ions in solution. The increased concentration of ions in solution compresses the diffuse layer and thus, decreases the distance the electrical potential field

extends from the particle surface, reducing the repulsive forces. The decreased size of the diffuse layer allows other particles to approach close enough to experience attractive van der Waals forces. If particles approach one another with sufficient kinetic energy to overcome the resultant net energy barrier, aggregation occurs. Thus, at low ionic strength, the rate of aggregation is limited by the large diffuse layer repulsive force. At the critical coagulation concentration (CCC) of ions, the aggregation rate no longer increases with increasing ionic strength because the diffuse layer has been maximally compressed and the energy barrier to collision has been eliminated. The regime of concentrations at and above the CCC are referred to as the diffusion-limited regime because only the rate of diffusion through the solution now limits the rate of aggregation. Concentrations below the CCC are referred to as the reaction-limited regime because there is still an energy barrier which must be overcome for aggregation. The interaction energy as a function of distance can be seen in Figure 2.

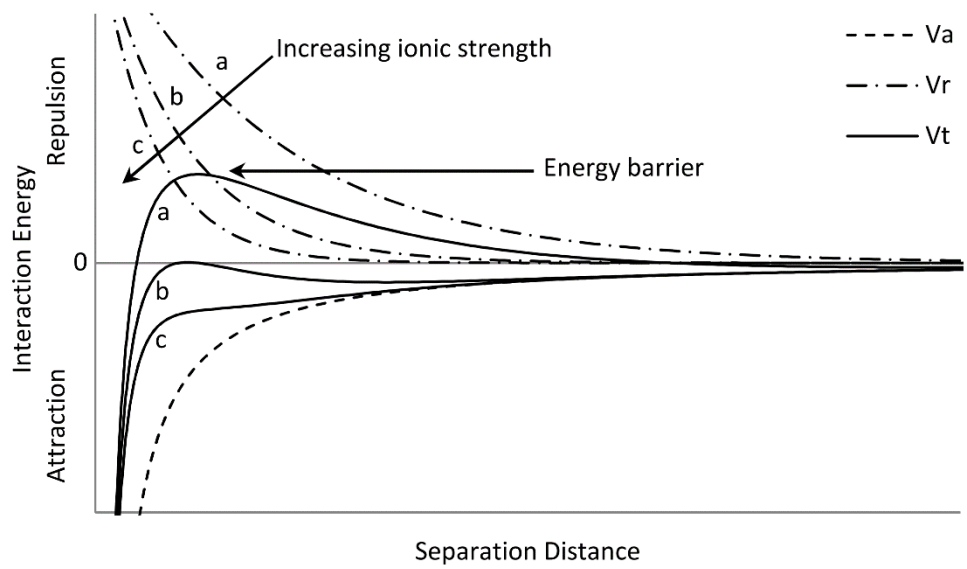

Figure 2. Energy of interaction for particles approaching one another in (a) the reaction-limited regime, (b) at the CCC, and (c) in the diffusion-limited regime. The attractive forces are V_a, the repulsive forces are V_r and the total energy of interaction is V_t.[9]

The Schultz-Hardy rule states that the destabilizing power of an electrolyte is principally due to the valence of its counterion to the colloidal particle surface.[10] The efficiencies of various electrolytes in destabilizing can be expressed in terms of a critical coagulation concentration.

$$CCC = \frac{constant}{z^6}$$

where z is the valence of the counterion. Therefore, counterions with greater valence are expected to have critical coagulation concentrations much lower than counterions with lower valence.

2.5 Quantifying Aggregation

Several analytical techniques exist to measure aggregation rates. Perhaps the most prevalent method is time-resolved dynamic light scattering (TR-DLS). DLS measures particle size using fluctuations in the scattered intensity which are in turn related to diffusion coefficients (a function of particle size). The use of DLS as a measurement technique has several advantages. First, the instrument (90 Plus Particle Size Analyzer from Brookhaven Instruments) has a size range of 1 nm to 6 μm, appropriate for nanoparticles and colloids. Second, the measurements are non-destructive and can occur in solution, which eliminates any concern over the alteration of particle characteristics during sample preparation. The measurements require minimal time to complete and can be automated by the instrument to occur in rapid succession to examine changes in the hydrodynamic diameter over time. DLS also has several disadvantages to its use. The DLS uses a hard sphere approximation, which may not well describe the behavior of irregularly shaped engineered nanoparticles. Because the scattering intensity is proportional to particle diameter to the sixth order, the average size measured is substantially skewed to larger particle diameters, producing an intensity-weight hydrodynamic diameter. DLS provides the most accurate results with a monodisperse suspension. Additionally, DLS measurements provide only an average hydrodynamic diameter, providing little information as to the distribution of particle sizes in solution. Perhaps its largest drawback is that fast aggregation is difficult to quantify because as the time for each measurement decreases, the accuracy of the measurement also decreases. TR-DLS is often used to calculate initial rates of aggregation

Nanoparticle tracking analysis (NTA) is another analytical technique to measure aggregation rate. NTA calculates particle size by analyzing the movement of particles in ultra-high-resolution video taken of laser light reflecting off the particles. NTA is also a non-destructive method which analyzes particle size in solution. NTA produces a number-weighted particle size distribution with a user-specified data resolution. However, it requires a longer measuring period to collect a limited number of particle tracks. Many particles must be tracked to create a size distribution, requiring a higher concentration than DLS. When there is a wide distribution in size, the smallest particles may not scatter enough light to be tracked. In addition, NTA also relies on a hard sphere approximation to estimate the size of the particle from the Brownian motion. Previous research in the Nason Lab has relied on the use of a Coulter Counter to determine the particle size distributions. However, the lower bound of its range was too large (0.4 μm) to measure particles in the nanoscale range. This investigation will explore the use of NTA for tracking nanoparticle aggregation.

2.6 Existing Mathematical Model

The current mathematical model, developed by Nason and Lawler in C++, is based upon the discretized Smoluchowski coagulation equation and particle interaction theories of rectilinear and curvilinear models. The model uses several assumptions inherent to the Smoluchowski coagulation equation:

1. Due to the infrequency of collisions of higher order, only binary collisions are considered.
2. All particles are assumed to be hard spheres (particle porosity neglected).
3. Aggregation events are assumed to result in particle that is also a hard sphere (coalescence).
4. Particle volume (and thus mass, because porosity is neglected) is conserved during collisions.
5. The three long-range transport mechanisms act simultaneously to cause aggregation.
6. Floc break-up is neglected.
7. The solution is assumed to be well-mixed.

The particle size domain was discretized into logarithmically-spaced bins to improve computational efficiency while maintaining sufficient resolution at small particle sizes. The system of equations was numerically integrated using Heun's predictor corrector method. Due to the low likelihood that particles will aggregate into the center of each particle size bin, weighted particle volumes were added to the standard sizes immediately above and below the intermediate size to conserve volume.

The model requires several types of inputs: suspension characteristics, reactor configuration, and model operation parameters. For suspension characteristics, the model requires temperature, viscosity, particle bulk density, and an initial particle size distribution. For reactor configuration, the model requires a velocity gradient and an attachment efficiency. The model operation parameters are the lower limit of the size range, number of size bins, bin spacing, integration minimum and maximum step size and a selection of which collision mechanisms are present.

3 Materials and Methods

3.1 Colloids and Nanomaterials

3.1.1 Hematite Colloids

The hematite (α-Fe_2O_3) colloids were synthesized via the forced hydrolysis of $FeCl_3$ procedure outlined in Smith et al.[11] and the mass concentration of the stock solution (384.0 mg L^{-1}) was determined by total suspended solid analysis and confirmed with a quantification of total iron.

3.2 Suspending Mediums

3.2.1 Potassium Chloride Solution

ACS-grade potassium chloride (KCl) was used to create a 3 M stock solution of KCl. The stock solution was then filtered (0.2 µm nylon; VWR) to remove any remaining suspended particles.

3.2.2 EPA Synthetic Freshwater

A stock solution of very hard EPA synthetic freshwater was prepared using calcium sulfate, magnesium sulfate, sodium bicarbonate and potassium chloride in distilled deionized (DDI) water with an electrical resistance of 18.2MΩ-cm (ELGA Purelab Ultra).[12] The stock solution was then filtered (0.2 µm nylon; VWR) to remove any remaining suspended particles.[13] All inorganic salts were ACS reagent-grade.

3.2.3 Willamette River Water

Willamette River water was collected during summer in Corvallis, Oregon. The water was filtered (0.2 µm nylon; VWR) to remove any suspended solids and natural colloids.

3.3 Time-Resolved Dynamic Light Scattering

Time-resolved dynamic light scattering (TR-DLS) was used to investigate the aggregation behavior of the particles. The aggregation behavior of each type of colloid was studied as a function of ionic strength in the monovalent electrolyte, KCl, and in polyvalent EPA standard synthetic freshwater.

3.1.1 Sample Preparation

To measure particle size via dynamic light scattering, samples were analyzed with a 90 Plus Particle Size Analyzer (Brookhaven Instruments). Particles were measured at an overall colloid concentration of 25 mg L^{-1} in 4 mL polystyrene cuvettes. Initial samples for particle sizing were prepared by diluting the hematite colloid stock solution with distilled deionized (DDI) water with an electrical resistance of 18.2MΩ-cm (ELGA Purelab Ultra). Prior to each use, the colloid stock solutions were sonicated for 1-2 minutes in a bath sonicator (BT500A-MTH, VWR). Initial intensity-weighted

hydrodynamic diameters (D_h) were calculated as the average of three one-minute runs. For TR-DLS, 120 fifteen-second measurements separated by one second were taken over approximately 32 minutes. Fifteen-second measurements were chosen as a reasonable compromise between accurate data readings and good data resolution, where longer measurement intervals generally yield more accurate results and shorter intervals yield greater resolution during periods of rapid aggregation. Sample preparation occurred in the following sequence: (1) a blank 3.5 mL sample was prepared and analyzed; (2) addition of colloid and DDI water; (3) initial size measurement via DLS; (4) addition of concentrated salt solution; (6) inversion of cuvette and immediate analysis via TR-DLS.

3.1.2 Initial Rate of Aggregation Calculation

The initial rate of aggregation was calculated as measured hydrodynamic diameter increased over time between the initial diameter (D_0) and the first measurement in which the measured diameter exceeded $1.3D_0$. This range of aggregation was determined to be the optimal measurement of the initial aggregation rate because at $1.3D_0$ sufficient doublets of primary particles and few to no higher order aggregates had been formed from the primary particles.[14] For the data shown below in Figure 3, the initial slope estimate for hematite in 150 mM KCl is shown.

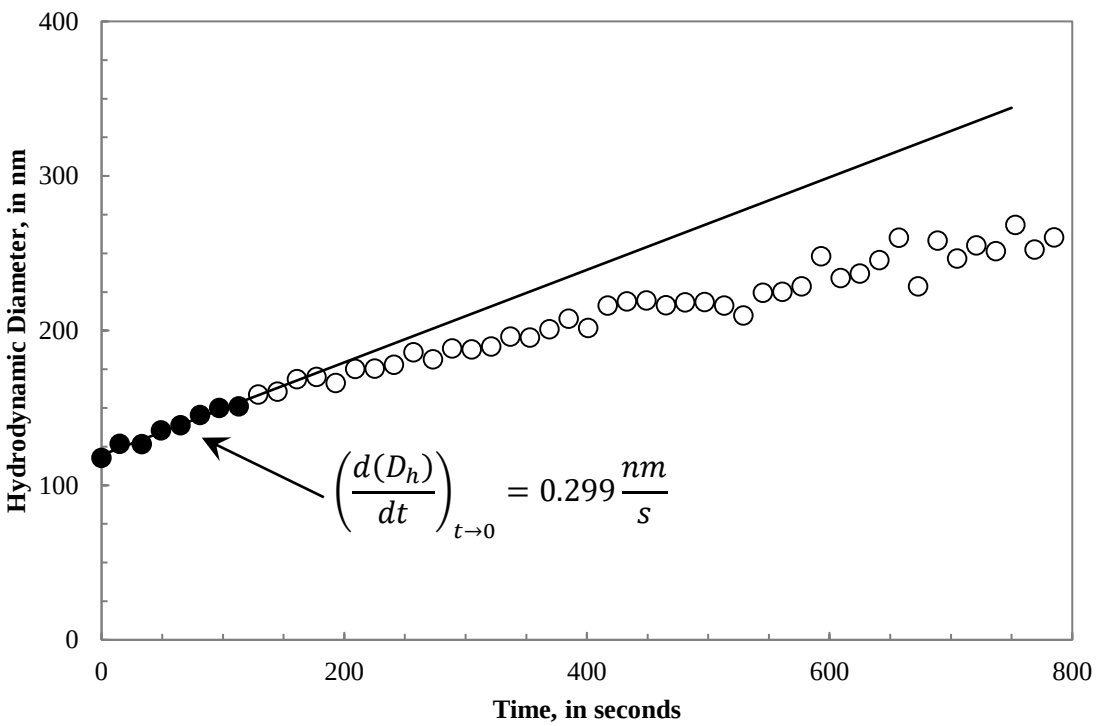

Figure 3. Calculation of the initial aggregation rate from TR-DLS measurements. Solid circles indicate data used to calculate the slope. Results shown are for synthesized hematite colloids in 150 mM KCl.

At fast aggregation rates, the TR-DLS does not allow for good resolution of data because the hydrodynamic diameter is measured over 15 second intervals and calculated slopes are based on very few data points.

3.1.3 Calculation of Attachment Efficiency (α_{emp}) and Critical Coagulation Concentration

The attachment efficiency was calculated from the initial aggregation rates according to the procedure outlined by Chen et al.[14] The rate of aggregation can be expressed as proportional to the absolute aggregation rate coefficient, see below.

$$\left(\frac{d(D_h)}{dt}\right)_{t\to 0} \propto k_{11}N_0$$

where D_h is the hydrodynamic diameter, k_{11} is the absolute aggregation rate between primary particles, and N_0 is the initial number concentration of primary particles.[15]

The attachment efficiency is the probability that an irreversible attachment will result from the collision of two colloidal particles. It is defined to be the absolute aggregation rate normalized to the aggregation rate under the most favorable conditions. The most favorable conditions occur when the rate of aggregation is only limited by the rate of diffusion of the particles in solution (diffusion-limited), as opposed to when the rate of aggregation is limited by the lack of availability of ions to compress the electrostatic diffuse layer (reaction-limited).

$$\alpha_{emp} = \frac{k_{11}}{k_{11,fast}} = \frac{\frac{1}{N_0}\left(\frac{d(D_h)}{dt}\right)_{t\to 0}}{\frac{1}{N_{0,fast}}\left(\frac{d(D_h)}{dt}\right)_{t\to 0,fast}}$$

For trials occurring at the same number concentration, the attachment efficiency can be simplified to:

$$\alpha_{emp} = \frac{\left(\frac{d(D_h)}{dt}\right)_{t\to 0}}{\left(\frac{d(D_h)}{dt}\right)_{t\to 0,fast}}$$

The critical coagulation concentration (CCC) represents the electrolyte concentration at which aggregation transitions from being reaction-limited to diffusion limited.

3.2 Nanoparticle Tracking Analysis

Nanoparticle tracking analysis was used to examine the changes in particle size distribution during aggregation. Trials were run in KCl solutions, and also in polyvalent EPA standard synthetic freshwater solutions.

3.2.1 Sample Preparation

The Nanoparticle Tracking Analysis (NTA) trials were prepared equivalently to the TR-DLS samples. Each sample was sonicated for 1-2 minutes immediately before measurement. A separate hematite sample at 25 mg L^{-1} was prepared in DDI water to represent an initial sample for all the trials.

NTA measurements were performed with a NanoSight NS500. The samples were pumped into the sample chamber via a peristaltic pump. All measurements were taken at 25 °C. The software used for capturing and analyzing the data on a linear scale was NTA 2.3. Select data was reanalyzed using NTA 3.1 to export on a logarithmic scale compatible with comparison to the model results. Samples were measured for 60 seconds. The camera level was standardized to 13 for all samples to minimize possible bias induced by varying parameters between samples. For each time measurement from the same sample, a new volume of sample was loaded from the 4 mL cuvette into the sample chamber.

Each sample measurement produced a histogram of particle concentration discretized with respect to particle diameter. The data was exported and a mass balance and further analysis was performed.

3.2.2 Mass Balance Calculations

Due to a wide discrepancy in the reported concentrations of data from the NanoSight NS500, the samples were internally normalized to the total mass concentration measured in each sample. The total concentration was determined by summing up the mass contributions of each particle size bin using the following formula:

$$C = \rho \sum_{i=1}^{n} \left(N_{c,i} V_{particle,i} \right) = \rho \sum_{i=1}^{n} \left(N_{c,i} \frac{1}{6} \pi {d_i}^3 \right)$$

where C is the total concentration, ρ is the bulk density of the material, $N_{c,i}$ is the number concentration of size i, $V_{particle,i}$ is the volume of an individual particle of size i, and d_i is the diameter of a particle of size i. The concentrations of individual size bins were then divided by the total mass concentration to find a percent frequency of each particle size occurring.

$$\%frequency = \frac{C_i}{C} = \frac{N_{c,i} V_{particle,i}}{\sum_{i=1}^{n} \left(N_{c,i} \frac{1}{6} \pi {d_i}^3 \right)}$$

This mass balance enables the direct comparison of the particle size distributions, which would otherwise be difficult to compare due to the mass discrepancy.

3.3 NTA Comparison to Model

To determine the model-estimated attachment efficiencies of the different experimental trials, all the mass concentrations of the experimentally measured particle size distributions were normalized to 25 mg L^{-1}. This was accomplished by dividing the number concentrations in each particle size bin by the measured concentration and multiplying by 25 mg L^{-1}, the actual added concentration. The initial measured size distribution was used in the model as the initial size distribution and the model was run using a variety of attachment efficiencies. The model generated particle size distributions at time increments of five minutes, matching the experimental data collected. The model-generated size distributions were compared with the experimentally-measured particle size distributions and a least sum of the squared error (LSSE) analysis for the particle concentrations was performed with respect to the attachment efficiency.

4 Results

This chapter is separated into four sections. The first section examines the aggregation of the hematite colloids in monovalent KCl and polyvalent synthetic freshwater via time-resolved dynamic light scattering. This is primarily to determine baseline aggregation behavior to determine optimal conditions for NTA testing. The second section examines changes in the particle size distribution of hematite during aggregation using NTA. The third section uses the particle size distribution data from the second section to determine the attachment efficiency. The fourth section discusses stiffness of the ODE system and the suitability of the numerical scheme and timestep.

4.1 Time-Resolved Dynamic Light Scattering.

In previously unpublished results, the critical coagulation concentration (CCC) of hematite in potassium chloride was estimated to be 0.068 M (see Appendix A2). The previous work was performed at a colloid concentration of 10 mg L^{-1}. Due to the dependence of the initial aggregation rate on the concentration of the colloid, the calculation of the critical coagulation concentration was repeated for trials with a concentration of 25 mg L^{-1} hematite, the minimum concentration at which the NanoSight instrument has an optimum number of particle tracks, allowing a direct comparison between the data sets. Running the TR-DLS trials at the higher concentration also allowed for a more accurate comparison between experimentally derived and modeled attachment efficiency. A wide range of KCl concentrations was used to ensure that data from both the reaction-limited and diffusion-limited regimes was collected.

Figure 4 shows the aggregation profiles of TR-DLS experiments with hematite colloids suspended in various concentrations of KCl. Hydrodynamic diameters prior to the addition of the KCl solutions had a measured average of 119 ± 5 nm (standard deviation, 9 replicates). At KCl concentrations at and above the CCC, it was expected that a maximum rate of aggregation would be reached, indicating that the system had entered a diffusion-limited regime. At concentrations below the CCC, the rate of aggregation was expected to increase linearly on a log-log scale with increasing concentration of KCl, indicating a reaction-limited regime. The data, shown in Figure 5, indicates a positive trend between the ionic strength and calculated attachment efficiency up to a certain concentration, consistent with DLVO theory. At low ionic strengths where electrostatic repulsion between the negatively charged particles creates a substantial energy barrier, the hematite is fairly stable. As the ionic strength is increased, the electrical double layer is compressed until the CCC is reached. At concentrations beyond the CCC, the hematite experienced no increase in initial aggregation rate. In Figure 5, plotting the attachment efficiency against KCl concentration and performing a linear regression of the reaction-limited regime reveals that the critical coagulation concentration of 25 mg L^{-1} hematite was approximately 33 mM KCl.

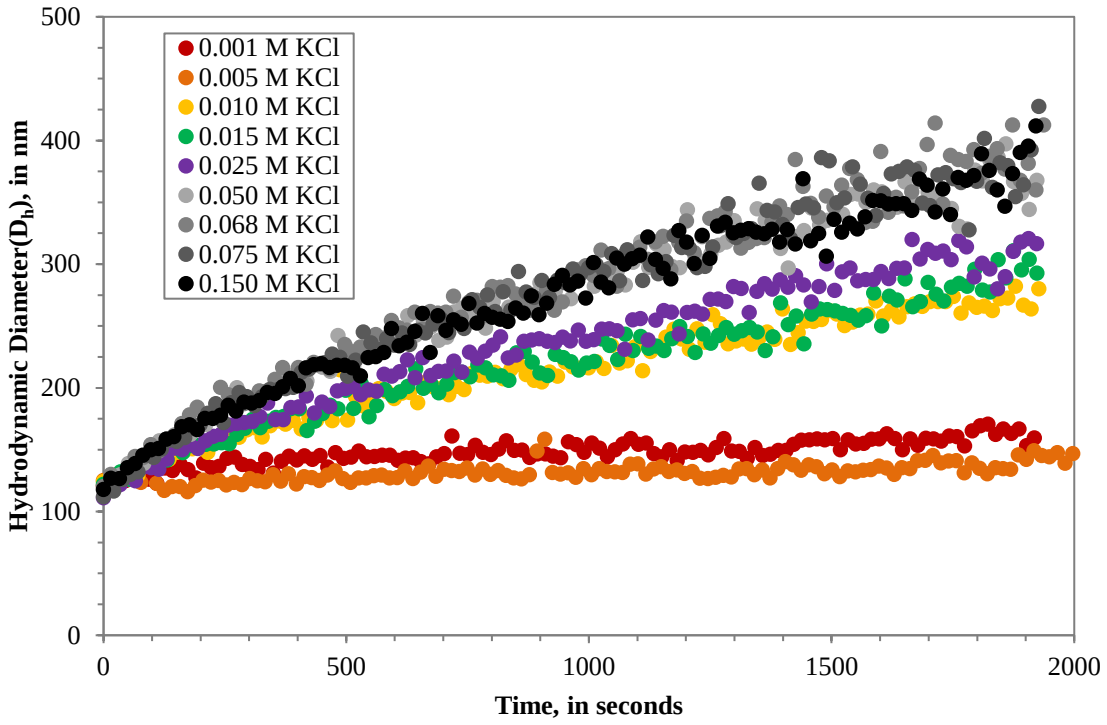

Figure 4. Intensity-weighted hydrodynamic diameter of hematite colloids in various concentrations of potassium chloride.

The linear regression of the data in Figure 5 indicated a slope of 30.6 M^{-1} in the reaction-limited regime. There appears to be substantial scatter of the data at the low end of the reaction-limited regime, but the actual variation of the initial aggregation rates can be seen to be quite small (see Appendix A1).

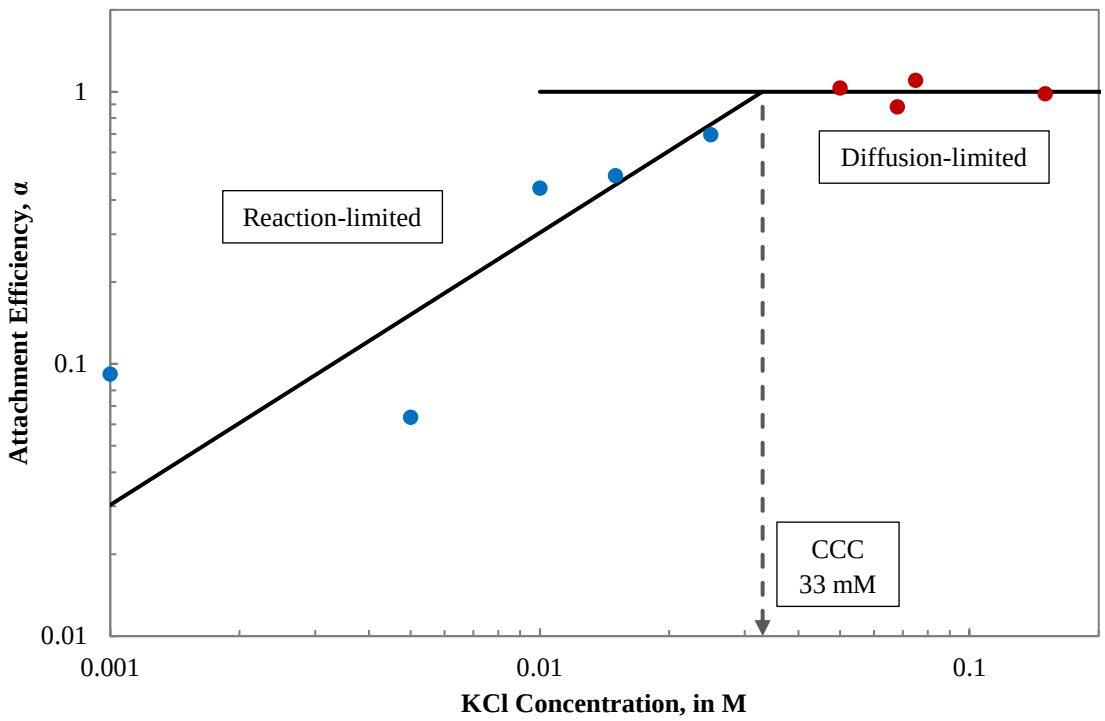

Figure 5. Attachment efficiencies for hematite colloids as a function of KCl concentration. The CCC calculated from the data is 33 mM KCl.

The $k_{11,fast}$ for 25 mg L^{-1} hematite was found to be 0.306 nm s^{-1}, compared to 0.414 nm s^{-1} for the 10 mg L^{-1} hematite. This indicates that the aggregation rates for the hematite was lower despite the higher colloid concentration. This disagrees with previous research which indicates that the rate of aggregation slows with a reduction in particle concentration.[16] However, the previous trials used a different stock solution of synthesized hematite, which, if there were any variations between the two synthesized batches, could impact the aggregation rate. The critical coagulation concentration was also found to be slightly lower on a log-log scale, 33 mM KCl compared to 68 mM KCl for the 10 mg L^{-1} hematite. However, given the number of data points that the CCC is based upon and the different stock solution used, this value is in reasonable agreement with the previously determined value.

Aggregation data were also collected for 25 mg L^{-1} hematite in EPA standard synthetic fresh water of various hardness, diluted from the very hard stock solution. A summary of the total ionic strength at the various EPA test water hardness is provided in Table 1. It is important to note that the ionic strength for the EPA test water is most strongly influenced by the presence of the divalent ions in solution, calcium sulfate and magnesium sulfate. In addition, the ionic strength of the very hard water was only 20 mM, just over half of the critical coagulation concentration of KCl. Figure 6 shows the aggregation profiles of time-resolved dynamic light scattering experiments with hematite suspended in EPA test water of varying water hardness.

Table 1. Ionic strength of EPA synthetic freshwater based on water hardness.

	Reagent Added (mg L^{-1})				Result	
	$NaHCO_3$	$CaSO_4$	$MgSO_4$	KCl	Ionic Strength, I (M)	pH
Very Soft	12.0	7.5	7.5	0.5	0.00062	6.4-6.8
Soft	48.0	30.0	30.0	2.0	0.0025	7.2-7.6
Moderately	96.0	60.0	60.0	4.0	0.0050	7.4-7.8
Hard	192.0	120.0	120.0	8.0	0.0099	7.6-8.0
Very Hard	384.0	240.0	240.0	16.0	0.020	8.0-8.4

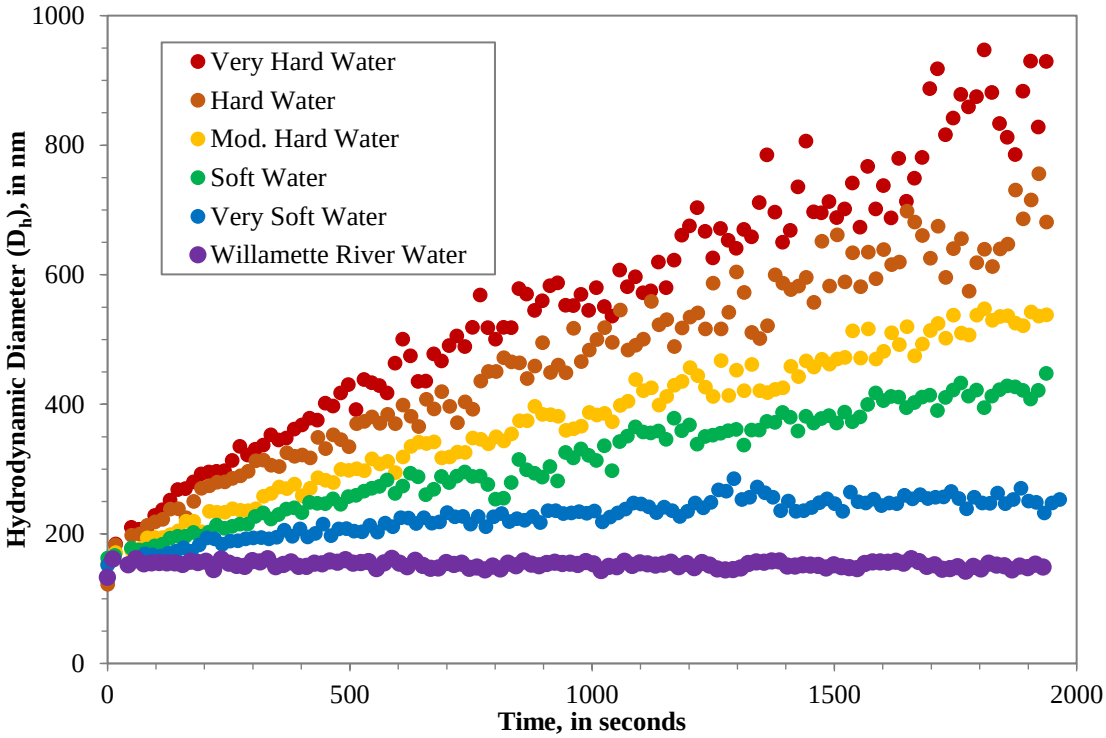

Figure 6. TR-DLS profiles of intensity-weighted D_h for 25 mg L^{-1} synthesized hematite during aggregation in various concentrations of EPA test water.

A comparison between Figure 4 and Figure 6 indicates that the hematite colloids aggregated substantially more in the very hard and hard EPA test water than in the KCl over the same time period. Hydrodynamic diameters prior to the addition of the salt solutions to modify water hardness were found to average 143 nm ± 17 nm (standard deviation, 5 replicates). Initial rates of aggregation were calculated for all samples except the Willamette River water, for which an aggregation rate was calculated over the whole trial because it never aggregated to $1.3D_{h,0}$. Initial rates of hematite aggregation ranged from 0.00 to 3.8 nm s^{-1} and increased with ionic strength, consistent with previous research and DVLO theory.[13] In the very soft water, electrostatic repulsion between the negatively charged particles creates a substantial energy barrier and the hematite is fairly stable. As the water hardness is increased, the electrostatic double layer is compressed, and more aggregation occurs. For hard and very hard EPA test

water, the hematite aggregated to 1.3$D_{h,0}$ within the first 15 seconds after the addition of the EPA test water. With ionic strength, the number of data points used to determine the aggregation rate decreases. This complicates the quantification and comparison of extremely fast aggregation because the rates measured exceed the resolution of the data. The Willamette River water sample experienced little to no aggregation, which is consistent with specific conductance measurements of the Willamette River during the sampling period indicating that the water was very soft.[17] One potential cause of the lack of aggregation in the Willamette River sample could be attributed to the presence of natural organic matter (NOM) in the solution, which, in previous unpublished results from the Nason lab, has been shown to raise the critical coagulation concentration in KCl. This is likely due to a low concentration of NOM increasing the stability of the hematite via surface-coating.[18] This agrees with previous unpublished results, which measured dissolved organic carbon (DOC) in the Willamette River on the order of 1 mg L^{-1}. However, due to changing weather and other factors, the DOC in the Willamette River sample used could be higher or lower.

The initial aggregation rates of the hematite in the standard synthetic freshwater were substantially higher than the aggregation rates measured in the trials with KCl. Previous data collected at 10 mg L^{-1} hematite indicated that the maximum aggregation rate in the divalent salt $CaCl_2$ was close to that in the monovalent KCl (0.425 compared to 0.414 nm s^{-1}). The CCC of $CaCl_2$ was lower than that of KCl, 0.016 M compared to 0.068 M. For a monovalent salt, the ionic strength is equal to the molar concentration. A divalent salt such as the $CaSO_4$ in the EPA test water would contribute four times more to the ionic strength than would monovalent KCl. The ionic strength for the CCC of $CaCl_2$ is 0.064 M, comparable to the ionic strength of KCl at the CCC, 0.068 M.

The EPA test water had a lower ionic strength than the trials of KCl and even the very hard water has a third lower ionic strength than the ionic strengths of the CCC for KCl and $CaCl_2$. Despite this, the hematite in the EPA synthetic freshwater experienced nearly ten times the rate of aggregation. This agrees with the Schultz-Hardy rule, which states that the destabilizing power of an electrolyte is principally due to the valence of its counterion to the colloidal particle surface. Because hematite has a positive surface charge under most environmentally relevant pH conditions, the valence of the negative ions in solution predominantly contribute to the aggregation rate. The divalent sulfate ions make up almost half of the number of counterions in solution, so we would expect faster aggregation and a lower CCC than for just the KCl.

The pH for the synthetic freshwater also increased as water hardness increased. Due to the protonation/deprotonation of hydroxyl surface groups on the colloids, the surface charge of the colloid is pH dependent. As pH increases, the hematite approaches its isoelectric point (pH = 9.7, where surface charge is zero), and the surface charge of the colloids decrease.[13] This decrease in surface charge reduces the electrostatic repulsive forces and allow for faster aggregation. On the other hand, the KCl trials were previously shown to be approximately pH 6,

farther from hematite's isoelectric point. The hematite in KCl would have a stronger surface charge and therefore more electrostatic repulsion.

4.2 Nanoparticle Tracking Analysis.

In addition to collecting data on the intensity-weighted hydrodynamic diameter via TR-DLS, nanoparticle tracking analysis was performed on some samples with a NanoSight NS500 to examine the changes in the particle size distribution over time. This data was primarily collected to allow for the estimation of the attachment efficiency via the least sum of squares analysis with comparison to the modelled data. Figure 7 shows the results of the nanoparticle tracking analysis experiment of hematite at 10-minute increments after the addition of moderately hard EPA test water.

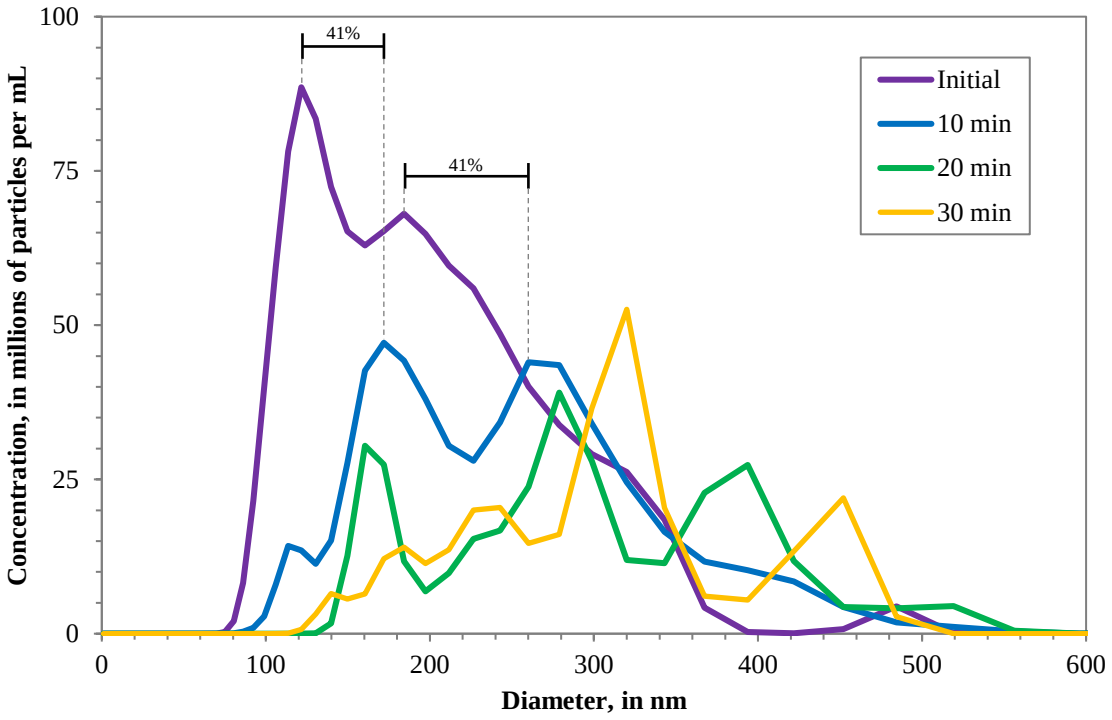

Figure 7. Number-weighted particle size distribution of hematite colloids in moderately hard EPA test water, measured using Nanoparticle Tracking Analysis.

Over time, the particle size distribution can be seen to shift toward larger particle sizes and broaden. The maximum number concentration also decreases as many smaller particles aggregate to form few large particles. This corresponds to an overall decrease in number concentration in the suspension.

The initial particle size distribution shows three distinct peaks, at 122 nm, 184 nm and 485 nm. The highest number concentration occurs at 122 nm, which is in good agreement with the effective hydrodynamic diameter measured via DLS (143 nm ± 17 nm st. dev.). Compared to the TR-DLS, NTA reports substantially less aggregation, with the NTA medians for the 4 time

points measured as 177, 267, 275 and 286 nm in order of time, compared with the 1-minute TR-DLS average at the same times being 154 308, 441 and 530, respectively. This is likely due to the intensity-weighting of the TR-DLS data, where intensity is proportional to diameter to the sixth power. The particle size distributions are not smooth, rather there are defined peaks at each time interval for different particle sizes. It can be observed that the mode of the concentration at 5 minutes is approximately 1.41 times the diameter of the concentration mode for the initial concentration sample. This is close to 1.38, the observed ratio between the effective hydrodynamic diameter of doublets to the effective hydrodynamic diameter of the primary particle.[19] As the time increases, more particle peaks appear at larger diameters representing doublets, triplets and other higher order aggregates. The peaks are generally spaced in such a way that a peak appears 30-50% above a previous peak. This behavior is consistent with current understanding of aggregation behavior. The distribution of particle sizes becomes wider as time progresses.

The total concentration of each sample was normalized to the added concentration, 25 mg L^{-1}. This normalization is necessary because the nanoparticle tracking analysis reports large differences in concentration in different measurements, even from the same sample. This is likely due to variations in the number of particle tracks between measurements. The difference between NTA calculated concentrations and actual concentration are shown below in Figure 8 for all hardness and times recorded. For the determination of mass concentration, the linear scale particle size distribution was used, with a particle size bin width of 1 nm. This allows for more accurate concentration calculation than the logarithmic scale data output, where bins get larger at the higher particle sizes, creating a larger calculation bias. The mass concentration in the solution should remain constant, but there are large discrepancies between measurements, even from the same solution.

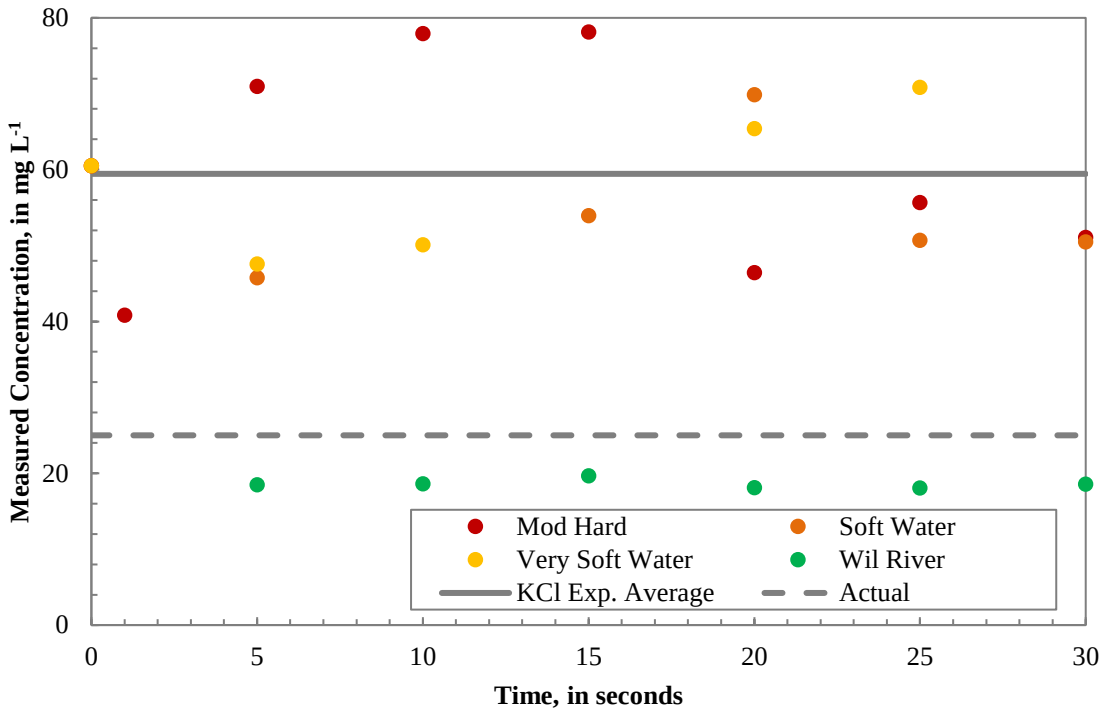

Figure 8. Comparison of the reported concentration of the various time measurements for hematite colloids in EPA test water. The KCl experiment average reports all samples prepared in KCl.

The average concentrations calculated from the particle size distributions of the hematite samples in DDI water was 59.4 mg L^{-1} ± 12.7 mg L^{-1}, more than double the 25.0 mg L^{-1} originally dosed in each sample. This is consistent with the results found by Mitrano et al. (2012) who found that while NTA exhibits a linear relationship between added concentration and measured concentration, the ratio is not necessarily 1:1.[20] In their trials with particles in DDI water, the scaling factor between the actual concentration and the measured concentration was approximately 3. The hematite sample in Willamette River only had an average concentration of 18.6 mg L^{-1} and a standard deviation of 0.57 mg L^{-1}. This discrepancy could potentially be attributed to the presence of NOM in Willamette River water. Mitrano et al. (2012) also found that for matrices with natural particles, the scaling factor was reduced to 2.[20]

Additionally, it is also possible that because the instrument uses the Brownian motion of the particles to estimate the particle size using a hard sphere assumption that NTA overestimates the size of aggregates. This might occur because the particles do not aggregate to hard spheres, but rather hematite has been observed to aggregate into a fractal structure.[21] This fractal structure increases the apparent size as it moves through solution, but its porous structure can also allow water to pass through the particle, which can reduce the water resistance. The hard sphere assumption relates the apparent diffusivity to a particle diameter using the Stokes-Einstein equation. If the fractal structure experiences less diffusion than a corresponding hard sphere of equivalent volume, nanoparticle tracking analysis will overestimate the particle size. This could be one reason why the reported mass is higher than the added mass. Therefore, it is

recommended, in agreement with previous research, that a calibration curve be made for each new matrix of interest to determine the scaling factor between the actual and the measured concentration.[20]

4.3 Experimental and Modelling Comparison

The experimental data analyzed in the previous section was compared to the model to determine if the model accurately predicted the aggregation behavior of the hematite. The particle size distributions from the NTA experiments were normalized to the expected concentration, 25 mg L^{-1} hematite, and compared to the model output that used the experimental initial size distribution. The model was run using the curvilinear model for Brownian motion, with aggregation from differential sedimentation and fluid shear neglected. These simplifications are appropriate for this system because there is no velocity gradient present in the sample and the particles are so small that it can be assumed that little sedimentation occurs during the 30 minute trials. A full summary of the model inputs used can be found in Appendix A3. In general, the model demonstrated a broadening of the particle size distribution and a reduction in number concentration, behavior consistent with the experimental data. Figure 9 compares the experimentally-determined initial size distribution with the model outputs at 10, 20 and 30 minutes for an attachment efficiency of 0.3.

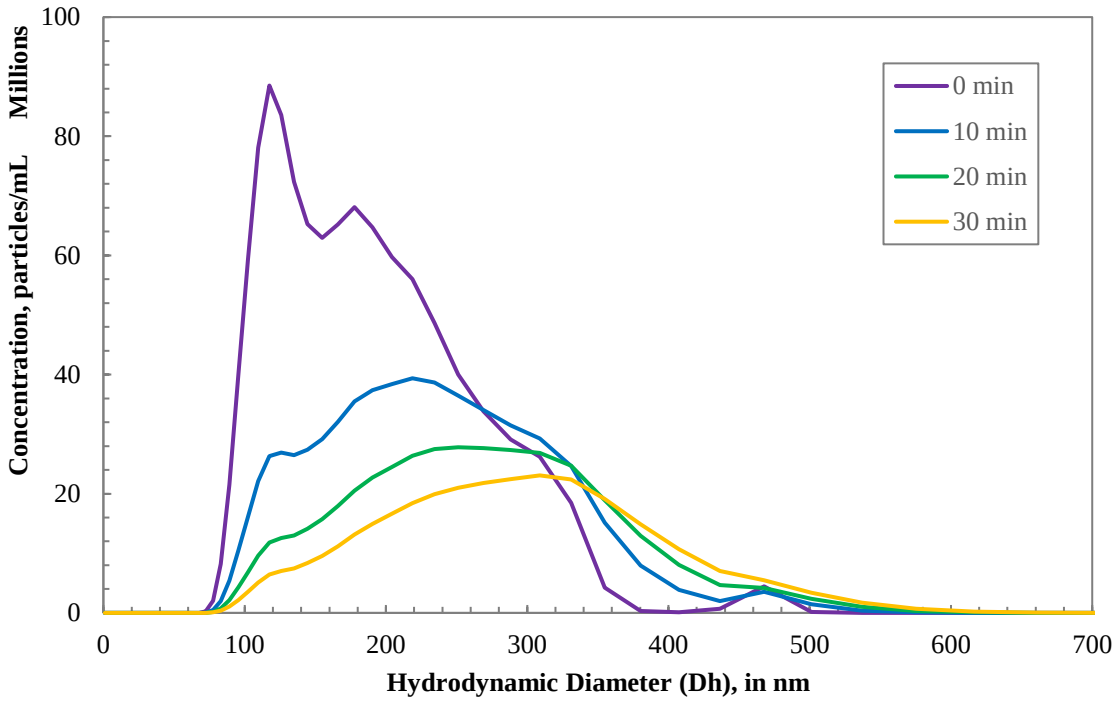

Figure 9. Particle size distributions of initial model input with time resolved particle size distribution outputs from the model.

Over the shortest time interval, 0 – 5 minutes, the model-estimated alpha values were 0, 0.35 and 0.675 ± 0.025 for very soft, soft and moderately hard water, respectively. The model-

estimated attachment efficiencies for 0 – 5 minutes are plotted with initial aggregation rate in Figure 10. This time interval was chosen because it most closely corresponds with the time intervals of initial aggregation measurements for TR-DLS (2.5 – 6 minutes). There is a strong linear correlation between the experimentally-measured initial aggregation rate and the model-estimated attachment efficiency.

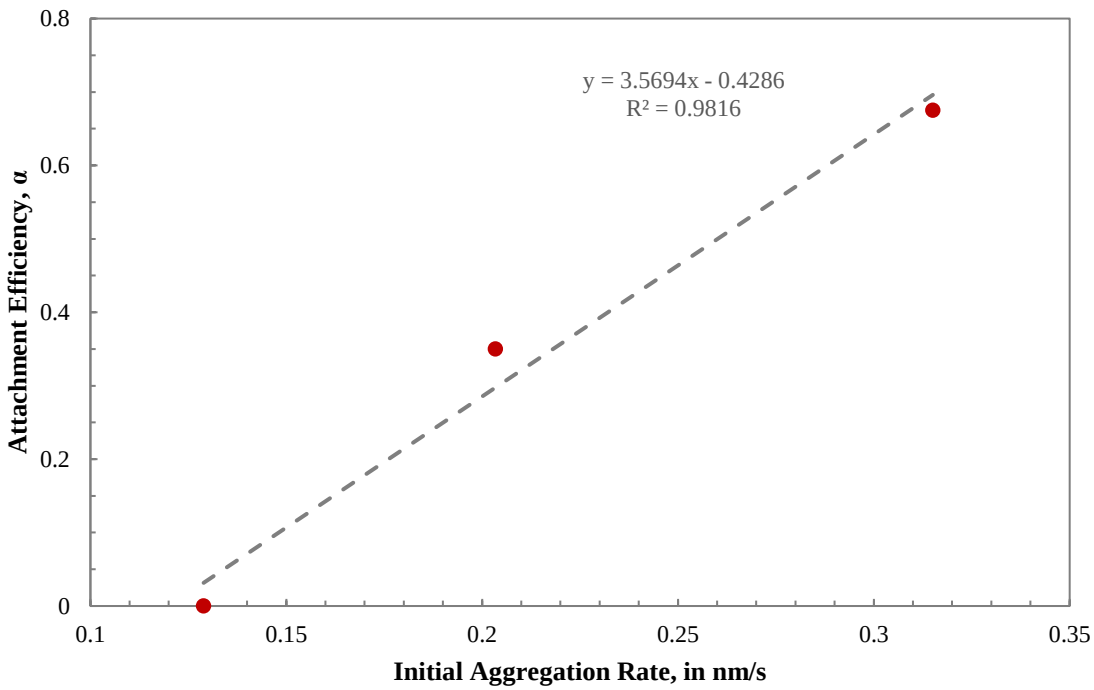

Figure 10. Comparison of model-estimated attachment efficiency with experimental initial aggregation rate.

The increasing attachment efficiency as water hardness increased indicates that aggregation was occurring in a reaction-limited regime, consistent with the aggregation behavior observed via TR-DLS. However, when the model output is compared to the experimentally-measured particle size distribution, the qualitative appearance of the two distributions differ substantially. Figure 11 shows a comparison between the experimental data and the model output using the best fitting attachment efficiency ($\alpha_{emp} = 0.45$) for moderately hard water at 20 minutes.

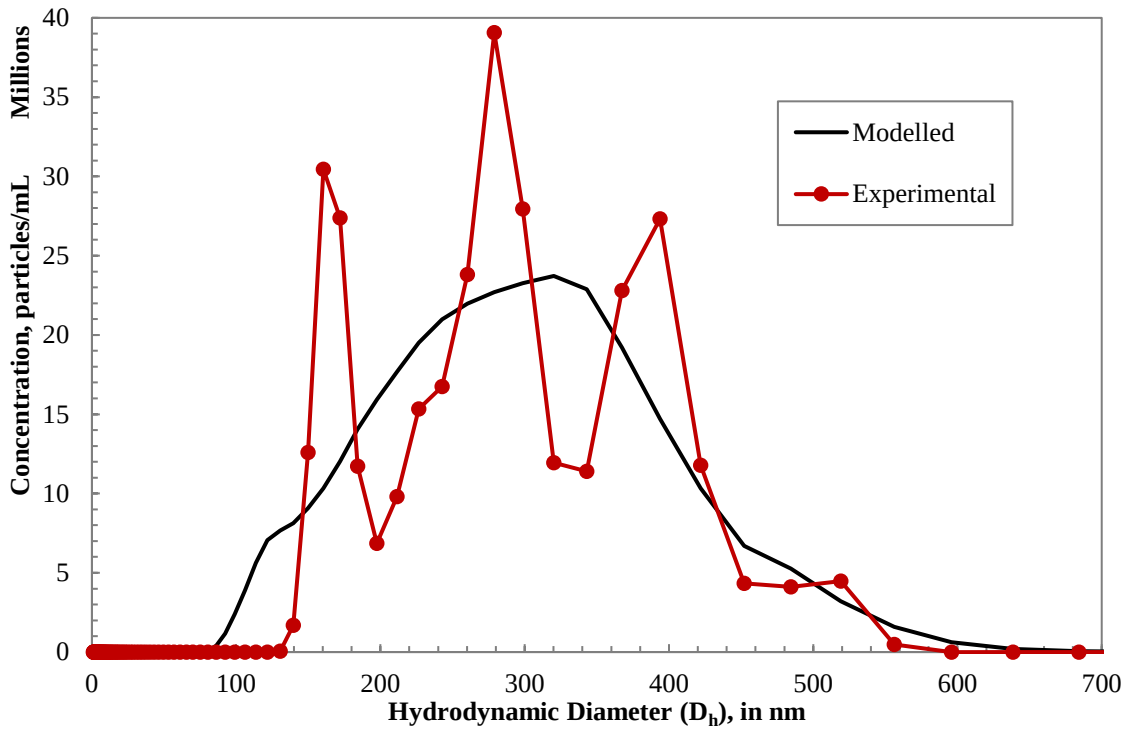

Figure 11. Comparison of experimental and modelled particle size distribution using $\alpha_{emp} = 0.45$ for moderately hard synthetic freshwater at 20 minutes.

The qualitative appearances of the particle size distributions differ substantially. The experimentally measure data has strong peaks at diameters corresponding to primary, doublet and higher order particles. The modelled data shows a smooth curve of concentration. This can be attributed primarily to the discretized nature of the model. Because the model is discretized on a logarithmic scale, the likelihood of two particles aggregating into the exact center of a larger size bin is unlikely. To conserve mass, the concentration of aggregates that would have fallen between two size bins contributed a concentration to each size bin based on the difference in volume between the lower and upper size bin. This way, fractions of particles are assigned to the smaller and larger size bins and mass is conserved. Over time, the higher order particles have wider peaks due to many of these mass-conservation events. Despite the smoothing behavior, the model does capture the general trend in the size distribution well.

The attachment efficiencies estimated over the first 10 minutes were used to predict the change in the particle size distribution from 10 to 30 minutes. This analysis was performed to identify if the model-estimated attachment efficiency could be used to predict the aggregation behavior over a longer time period. If there is good agreement with the modelled and experimental distributions at 30 minutes, it indicates that the model accurately reflects the behavior. It also indicates the viability of using NTA in tandem with the model to predict aggregation. The time interval 0 – 10 minutes was chosen as the shortest time interval where all samples had a non-zero model-estimated attachment efficiency. The results for the predicted distribution and the actual distribution are located in Figure 12. For the very soft water, the

model underpredicted the aggregation. The size peaks were also slightly smoothed. For the soft water, the model overpredicted the aggregation. There were clear size peaks, however, they were smaller due to the increased aggregation. For moderately hard water, the model also overpredicted the aggregation. The particle size distribution was also noticeably smoothed.

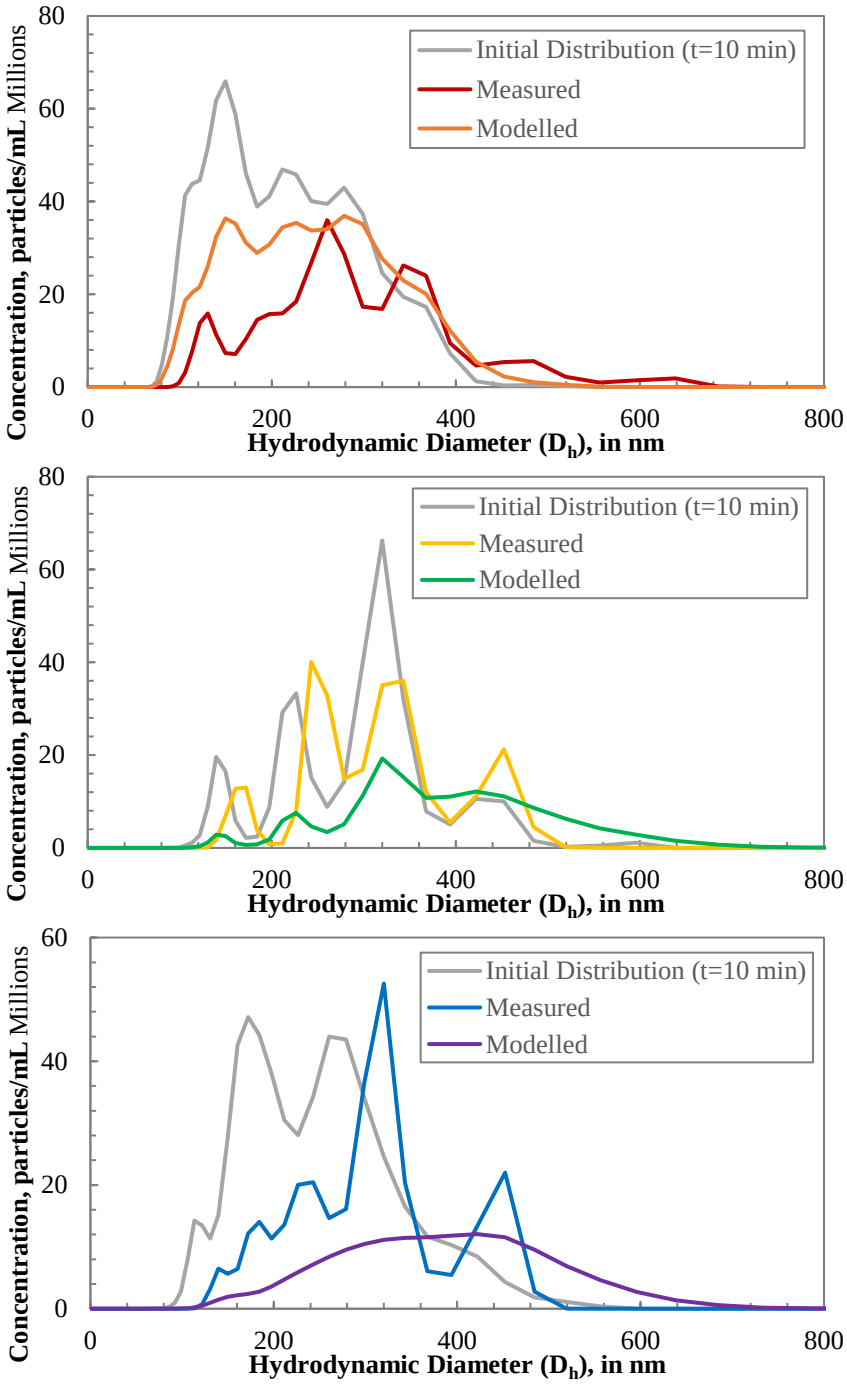

Figure 12. Comparisons of experimental results at 30 minutes with the model prediction from 10 to 30 minutes, using the attachment efficiency estimated from 0 to 10 minutes and the experimental distribution at t=10 min as the initial input for the model for (a) very soft water, (b) soft water, and (c) moderately hard water.

Because of the discrepancies between the measured and modelled particle size distributions, the best-fitting attachment efficiencies from $t = 0$ to each time step were calculated. The attachment efficiencies were estimated using the least sum of the squared error between the measured and modelled number concentrations at each time. The best fitting attachment efficiencies were not constant over these intervals, as shown in Figure 13.

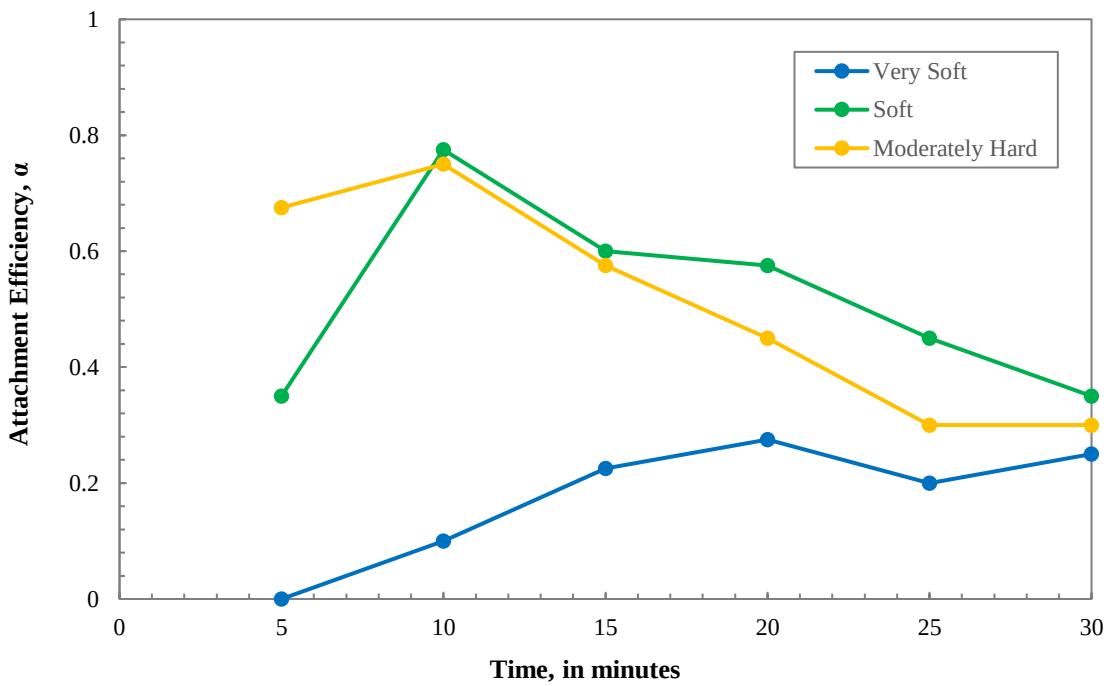

Figure 13. Model-estimated attachment efficiency based on time interval of comparison.

Between 5 and 10 minutes, the model-estimated attachment efficiency increased for all samples. However, between 10 and 30 minutes, the attachment efficiencies for soft and moderately hard water decreased steadily while the attachment efficiency for the very soft trial mostly increased. Moreover, after ten minutes, the soft water sample consistently had a higher attachment efficiency than the moderately hard water sample. This disagrees with the results from TR-DLS and from the NanoSight, which showed that aggregation rate increased with increasing ionic strength. It is possible that, due to the smoothness of the modelled distributions in comparison to the experimental data, a LSSE analysis on the concentration is not an appropriate method for finding the best-fitting alpha. For future work, it is recommended that an investigation occur comparing the results of a LSSE analysis on the concentration with an LSSE analysis on the particle size distribution function ($\log(dN/dd_p)$).

If the model completely captured the behavior of the system and the NTA data was entirely accurate, then the attachment efficiency would remain the same for all thirty minutes. The variation in attachment efficiencies over the time interval is indicative of two issues. First, the model may not mechanistically account for some factors, which makes the attachment

efficiency change over time. This is possible because the model does not directly account for electrostatic repulsion, particle geometry or aggregate breakup. The increased likelihood of aggregate breakup as aggregate size increases is a known phenomenon, though this is most significant under a velocity gradient. In addition, electrostatic repulsion has not been observed to change significantly with aggregation. The neglect of considering particle porosity in the model should cause the model to underpredict aggregation as aggregation progresses, not overpredict. The most likely cause is aggregate breakup.

The second issue is that NTA may not accurately measure particle size distributions. This is a potential concern because of the low number of particles sampled. While a sample may have up to 9000 successful particle tracks, the number of unique particles tracked is much lower. The number of particles tracked is a product of the size of the viewing pane and the narrow focus depth of the camera. Additionally, large particles produce brighter scatter, and could potentially drown out the scattering of smaller particles. Also, by the nature of aggregation, there is a reduction of particle number concentration over time, which further reduces the number of particles present in the viewing window. This change can be seen in Figure 14.

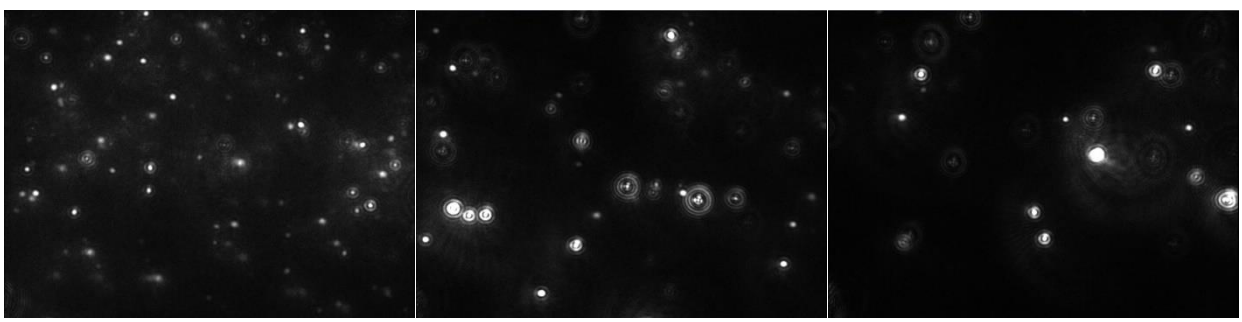

Figure 14. Screenshots from NTA of hematite colloids in 68 mM KCl: at (a) $t = 0$ min, (b) $t = 15$ min, and (c) $t = 30$ min.

By 30 minutes, only a few particles are left in the viewing window, making the extrapolation of the particle size distribution less accurate. This calls into question the accuracy of particle size distributions measured via this method. One potential improvement could be to increase the time of the video analysis. This could increase the number of particles seen, but it also reduces the resolution of the data with respect to time. Additionally, due to the lack of a velocity gradient, it is likely that particles will stay within the viewing window instead of more particles being sampled. Another solution could be to perform multiple samples and average the particle size distributions. This would sample more particles at the same time without sacrificing data resolution but take substantially more time and resources. Repeated measurements of a single sample of nanoparticles should be performed to determine the variability between measurements. A comparison of the average size distribution with a distribution from a longer video analysis could shed light on which of these methods may be more useful.

In addition, it may be helpful to reanalyze existing data using a finer size bin width. This will be more computationally intensive for the model but will also reduce the smoothing behavior of the model and allow a better fit between the experimental data and the model output.

4.4 Modelling Considerations

The Smoluchowski coagulation equation, shown below, is a population balance equation which describes the time evolution of the concentration of particles of size *k* at time *t*.

$$^{Flocculation}r_k = \frac{dN_k}{dt} = \frac{1}{2}\alpha_{emp} \sum_{\substack{all\ i\ and\ j \\ such\ that \\ V_i+V_j \\ =V_k}} \gamma_{ij} N_i N_j - \alpha_{emp} N_k \sum_{all\ i} \gamma_{ij} N_i$$

where: $\gamma_{ij} = {}^{Br}\alpha_{ij}{}^{Br}\beta_{ij} + {}^{Sh}\alpha_{ij}{}^{Sh}\beta_{ij} + {}^{DS}\alpha_{ij}{}^{DS}\beta_{ij}$

As the number of particle size bins increases, the number of binary size combinations of potential aggregation events increases on the order of $\frac{n^2+n}{2}$. Due to the complexity and nonlinearity of the ODE system, predicting particle size distribution over time via analytical integration is infeasible. The model developed by Nason and Lawler[3] uses Heun's method for solving non-stiff differential equations and Gear's method for solving stiff differential equations. However, the model only employs Gear's method when the terms for particle nucleation and precipitation are accounted for (not shown in the equation above). However, due to the dependence of both the alpha and beta terms on colliding particles' diameters, the gamma coefficient varies depending on the combination of particle sizes.

4.4.1 Investigations of System Stiffness

One outcome of this investigation is to evaluate the stiffness of the system of ordinary differential equations. A system of ODEs is called stiff when the Jacobian matrix of a system has eigenvalues with large discrepancy in magnitude.[22] A large stiffness ratio, defined to be $L = \frac{max|Re(\lambda_i)|}{min|Re(\lambda_i)|}$ of the Jacobian, indicates that there is a wide range of time scales present in the problem. In practice, difficulties arise when attempting to numerically solve the initial value problem because many numerical methods, including all explicit methods, are not sufficiently stable, "unless the time step is small relative to the time scale of the rapid transient".[22] Sufficiently stable means that a large timestep can be used to solve the problem. Thus, determining system stiffness is essential to identifying the optimum finite difference method and time step for the numerical solution. To begin, the Jacobian of a system must be calculated.

A size three test system was used to study the issues before the full system is examined. Maximum, minimum and median values for the γ_{ij} constants were used to represent the interactions between the particle sizes, to capture variabilities that are

expected to appear in a real system. The system is shown below. The system is discretized with respect to particle volume where the particle volume of a size n+1 particle is double the volume of a size n particle.

$$\begin{pmatrix} r_1(t,N_1,N_2,N_3) \\ r_2(t,N_1,N_2,N_3) \\ r_3(t,N_1,N_2,N_3) \end{pmatrix} = \begin{pmatrix} \frac{dN_1(t)}{dt} \\ \frac{dN_2(t)}{dt} \\ \frac{dN_3(t)}{dt} \end{pmatrix} = \alpha_{emp} \begin{pmatrix} -\gamma_{11}{N_1}^2 - \gamma_{12}N_1N_2 - \gamma_{13}N_1N_3 \\ \frac{1}{2}\gamma_{11}{N_1}^2 + \left[\frac{1}{2}\left(\frac{1}{2}\right)\gamma_{21}N_2N_1\right] - \gamma_{21}N_2N_1 - \gamma_{22}{N_2}^2 - \gamma_{23}N_2N_3 \\ \frac{1}{2}\gamma_{22}{N_2}^2 + \left[\frac{1}{2}\left(\frac{1}{2}\right)\gamma_{21}N_2N_1\right] - \gamma_{31}N_3N_1 - \gamma_{32}N_3N_2 - \gamma_{33}{N_3}^2 \end{pmatrix}$$

This system reflects all the potential aggregation combinations possible. The terms listed in brackets correspond to a mass balance which accounts for the fact that an aggregate consisting of one particle of size 1 and one particle of size 2 aggregates to a volume that is halfway between particle sizes 2 and 3. The terms allocates half of the estimated concentration to the higher particle size class and half to the lower particle size class to conserve mass in the system.

The Jacobian, defined to be,

$$J = \alpha_{emp} \begin{bmatrix} \frac{\partial(r_1)}{\partial N_1} & \cdots & \frac{\partial(r_1)}{\partial N_n} \\ \vdots & \ddots & \vdots \\ \frac{\partial(r_n)}{\partial N_1} & \cdots & \frac{\partial(r_n)}{\partial N_n} \end{bmatrix}$$

For the test case discussed above, the Jacobian looks like the following:

$$J = \alpha_{emp} \begin{bmatrix} -2\gamma_{11}N_1 - \gamma_{12}N_2 - \gamma_{13}N_3 & -\gamma_{12}N_1 & -\gamma_{13}N_1 \\ \gamma_{11}N_1 - \frac{3}{4}\gamma_{21}N_2 & -\frac{3}{4}\gamma_{21}N_1 - 2\gamma_{22}N_2 - \gamma_{23}N_3 & -\gamma_{23}N_2 \\ \frac{1}{4}\gamma_{21}N_2 - \gamma_{31}N_3 & \gamma_{22}N_2 + \frac{1}{4}\gamma_{21}N_1 - \gamma_{32}N_3 & -\gamma_{31}N_1 - \gamma_{32}N_2 - 2\gamma_{33}N_3 \end{bmatrix}$$

Even for the size three test system, the Jacobian matrix is intricate and depends on the concentrations of the various particle sizes, which change over time. These dependencies make calculating the eigenvalues too complex to use the most common method, $\det(J - \lambda I) = 0$. Because the stiffness of the system is determined by the eigenvalues, the stiffness of the system is dependent on the concentration of particles in the various size bins. A simplification of the non-linear system is necessary to allow for the estimation of the system stiffness. The system can be simplified through linearization, which can help determine the behavior of solutions near equilibrium points. Equilibrium points of dynamical systems are defined to be time-independent solutions of the ODE system, as shown below.

$$\begin{pmatrix} r_1(t, N_1, N_2, N_3) \\ r_2(t, N_1, N_2, N_3) \\ r_3(t, N_1, N_2, N_3) \end{pmatrix} = \begin{pmatrix} \dfrac{dN_1(t)}{dt} \\ \dfrac{dN_2(t)}{dt} \\ \dfrac{dN_3(t)}{dt} \end{pmatrix} = \begin{pmatrix} 0 \\ 0 \\ 0 \end{pmatrix}$$

Given that concentration can only be a non-negative real number, an examination of r_1 demonstrates that the only trivial solution occurs when $N_1 = 0$. From r_2, it follows that if $N_1 = 0$, then N_2 must also equal zero. Lastly, if $N_1 = N_2 = 0$, then r_3 is only zero if $N_3 = 0$. Therefore, the only equilibrium of the system occurs when the concentrations of all three size bins are zero.

To linearize the system about the equilibrium, the nonlinear terms can be expanded using a Taylor series, shown below for a multivariable quadratic function, with $\boldsymbol{x}$ a column vector and $\boldsymbol{x_0}$ the point at which the Taylor series is expanded.

$$f(\boldsymbol{x}) = f(\boldsymbol{x_0}) + \nabla f(\boldsymbol{x_0})(x - \boldsymbol{x_0}) + \frac{1}{2}(\boldsymbol{x} - \boldsymbol{x_0})H_f(\boldsymbol{x_0})(\boldsymbol{x} - \boldsymbol{x_0})$$

About a point defined to be $N_1^\circ, N_2^\circ, N_3^\circ$, the Taylor expansion of our twice differentiable system takes the following form, where tilde denotes the expanded form.

$$\begin{pmatrix} \tilde{r}_1 \\ \tilde{r}_2 \\ \tilde{r}_3 \end{pmatrix} = \alpha_{emp} \times \begin{pmatrix} -\gamma_{11}\left(N_1^{\circ 2} + 2N_1^\circ(N_1 - N_1^\circ)\right) - \gamma_{12}\left(N_1^\circ N_2^\circ + N_1^\circ(N_2 - N_2^\circ) + N_2^\circ(N_1 - N_1^\circ)\right) - \gamma_{13}\left(N_1^\circ N_3^\circ + N_1^\circ(N_3 - N_3^\circ) + N_3^\circ(N_1 - N_1^\circ)\right) \\ \frac{1}{2}\gamma_{11}\left(N_1^{\circ 2} + 2N_1^\circ(N_1 - N_1^\circ)\right) - \frac{3}{4}\gamma_{21}\left(N_1^\circ N_2^\circ + N_1^\circ(N_2 - N_2^\circ) + N_2^\circ(N_1 - N_1^\circ)\right) - \gamma_{22}\left(N_2^{\circ 2} + 2N_2^\circ(N_2 - N_2^\circ)\right) - \gamma_{23}\left(N_2^\circ N_3^\circ + N_2^\circ(N_3 - N_3^\circ) + N_3^\circ(N_2 - N_2^\circ)\right) \\ \frac{1}{2}\gamma_{22}\left(N_2^{\circ 2} + 2N_2^\circ(N_2 - N_2^\circ)\right) + \frac{1}{4}\gamma_{21}\left(N_1^\circ N_2^\circ + N_1^\circ(N_2 - N_2^\circ) + N_2^\circ(N_1 - N_1^\circ)\right) - \gamma_{31}\left(N_1^\circ N_3^\circ + N_1^\circ(N_3 - N_3^\circ) + N_3^\circ(N_1 - N_1^\circ)\right) - \gamma_{32}\left(N_2^\circ N_3^\circ + N_2^\circ(N_3 - N_3^\circ) + N_3^\circ(N_2 - N_2^\circ)\right) - \gamma_{33}\left(N_3^{\circ 2} + 2N_3^\circ(N_3 - N_3^\circ)\right) \end{pmatrix}$$

The Jacobi matrix for this linearized test system is:

$$\tilde{J} = \alpha_{emp} \begin{bmatrix} -2\gamma_{11}N_1^\circ - \gamma_{12}N_2^\circ - \gamma_{13}N_3^\circ & -\gamma_{12}N_1^\circ & -\gamma_{13}N_1^\circ \\ \gamma_{11}N_1^\circ - \dfrac{3}{4}\gamma_{21}N_2^\circ & -\dfrac{3}{4}\gamma_{21}N_1^\circ - 2\gamma_{22}N_2^\circ - \gamma_{23}N_3^\circ & -\gamma_{23}N_2^\circ \\ \dfrac{1}{4}\gamma_{21}N_2^\circ - \gamma_{31}N_3^\circ & \gamma_{22}N_2^\circ + \dfrac{1}{4}\gamma_{21}N_1^\circ - \gamma_{32}N_3^\circ & -\gamma_{31}N_1^\circ - \gamma_{32}N_2^\circ - 2\gamma_{33}N_3^\circ \end{bmatrix}$$

The Taylor series expansion shows that within a close range of the equilibrium point, the stiffness of the system is approximated by the Jacobian of the equilibrium conditions. However, due to the only equilibrium of the system occurring at zero, the Jacobian of the system is a null matrix. A null Jacobian matrix indicates that there is no change in concentration. However, from the differential equation, if any concentration is non-zero, there will be aggregation over time. Therefore, the linearization of the system of differential equations is not useful to understand the behavior of the system.

To get a better understanding of the stiffness of the system, the Jacobian and stiffness ratio of the size three system was evaluated on a uniform mesh using MATLAB. The mesh spacing was 5×10^6 particles/mL between 0 and 10^8 particles/mL. Gamma values corresponding to size 1 as 100 nm, size 2 as 126 nm, size 3 as 156 nm were used for the test system.

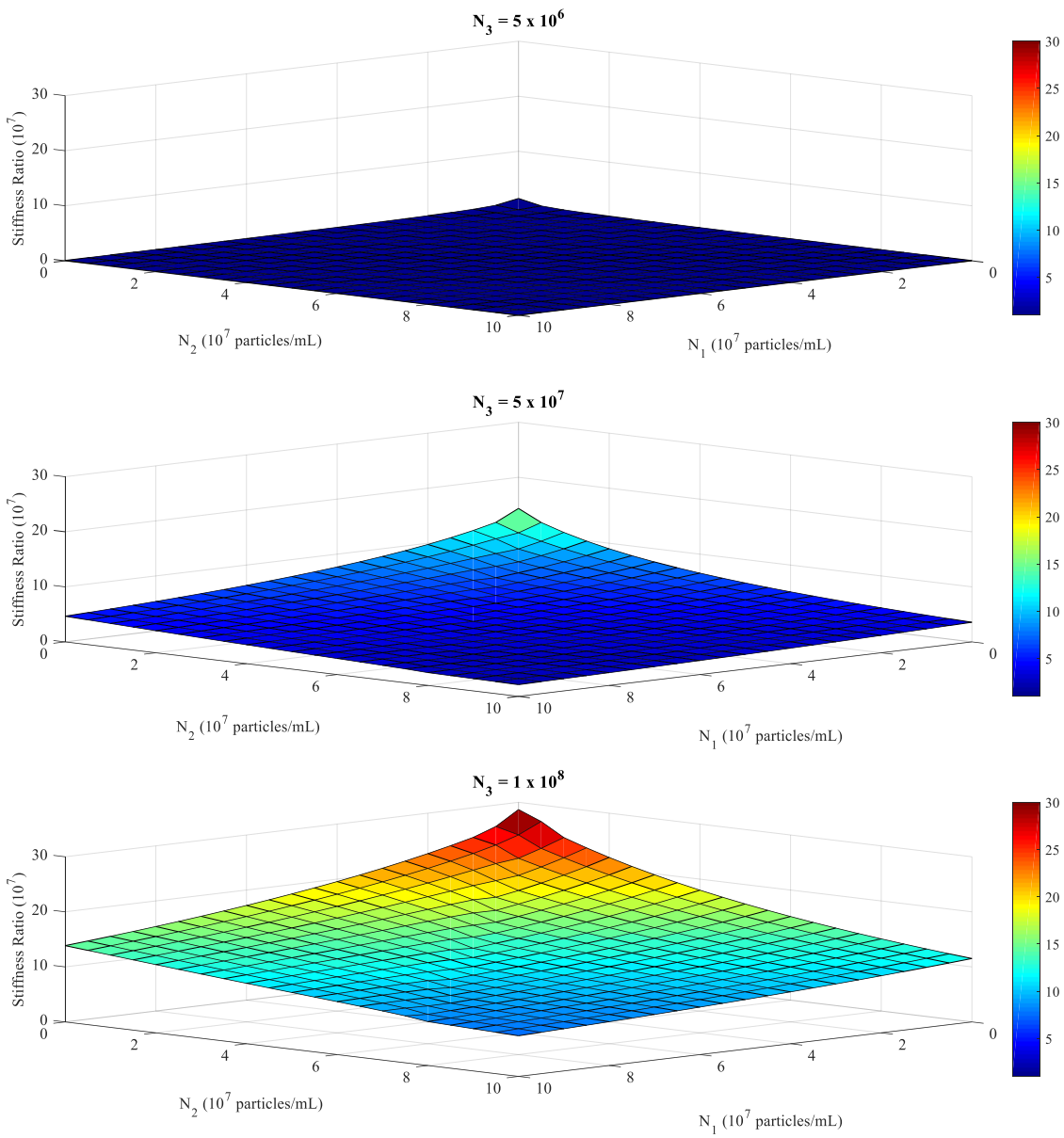

Figure 15. Stiffness ratios of the system at constant N_3 concentrations of $N_3 = 5 \times 10^6$, 5×10^7 and 1×10^8 particles mL^{-1} with N_1 and N_2 concentrations varying between 0 particles mL^{-1} and 1×10^8 particles mL^{-1}. The stiffness ratio is in units of 10^7 particles

The stiffness ratio was smallest when N_1 and N_2 were high and N_3 was low. This makes sense because the gamma coefficient, γ_{ij}, is largest when the size i and size j

greatly differ in size. However, it must noted that all combinations including a nonzero concentration of size 3 resulted in stiffness ratios of at least 10^7. This indicates that the size three test system is very stiff at nearly all points. To determine if this stiffness was a product of the three size system, the complexity of the system was expanded to include a fourth size, 200 nm, and utilized the accompanying gamma values.

With the size 4 test system, the stiffness ratios of the system were even higher. This is likely due to the larger difference between the largest size and smallest size, which increases the collision frequency function. Because both of these systems experience high stiffness, it is reasonable to assume that a similar system with increased complexity would also be very stiff.

The model based on Smoluchowski's coagulation equation currently uses Heun's method as the numerical scheme. Heun's method is the two-stage explicit Runge-Kutta method given by:

$$U^{n+1} = U^n + kf\left(U^n + \frac{1}{2}kf(U^n)\right)$$

This method has a region of absolute stability where the scheme is always stable, represented by:

$$R^{ABS} = \left\{z\colon \left|1 + z + \frac{z^2}{2}\right| \leq 1\right\}$$

For a numerical approximation of system of ordinary differential equations to be stable, the quantity $z = h\lambda$, where h is the step size in time and λ are the eigenvalues of system, must be in the region of absolute stability for all eigenvalues λ. For systems with a large difference in eigenvalues, such as this system, the maximum timestep is determined by the largest eigenvalue. In this system, λ_1 is predominantly on the order of 10^5. In order to operate the numerical scheme within its region of absolute stability, z must be between 0 and -2, so the time step must be on the order of 2×10^{-5}. This fine of a time step leads to computation that is very intensive. It is recommended that a numerical scheme with a larger region of absolute stability be implemented, ideally one that is A-stable. Numerical schemes that should be investigated are Backward Euler and backward differentiation.

5. Conclusion

The current study investigated the interactions of hematite in various electrolyte solutions, the comparability of experimentally-calculated attachment efficiencies with model-estimated attachment efficiencies, and the suitability of the numerical scheme for the solution of the Smoluchowski equation. The following conclusions can be drawn from the investigations and literature reviewed.

- Initial rates of aggregation of hematite in various concentrations of KCl increased with increased ionic strength, in agreement with DLVO theory.
- The CCC for KCl with 25 mg L^{-1} hematite colloids is approximately 33 mM.
- Aggregation rates in polyvalent synthetic freshwater are significantly faster than in the monovalent KCl and divalent $CaCl_2$. This indicates that environmentally, colloids may experience more rapid sedimentation than previously estimated by trials in KCl.
- At 5 minutes, model-estimated attachment efficiency had a strong correlation with measured initial aggregation rates.
- A LSSE analysis of the modelled and measured concentrations yielded model-estimated attachment efficiencies that varied over time.
- The reduced size 3 test system was found to be stiff at all non-zero concentration combinations of N_1, N_2, and N_3. This has large implications on the model because it currently runs on a numerical scheme that does not operate well on stiff systems.

The following is a list of areas where the scope of the work can be broadened to create a better union between experimental studies and modelling of aggregation.

- Experimental trials to estimate the CCC of hematite in synthetic freshwater should be performed so a comparison with KCl can be made.
- Nanoparticle tracking analysis should be performed on hematite in KCl, which is a more characterized system for modelling comparison.
- There are several investigations that must occur before continuing with the comparison between model outputs and NTA results.
    - First, the replicates of particle size distributions should be taken to determine the variability of a single time measurement.
    - Secondly, trials should be run in replicate to collect enough unique particle tracks to generate an accurate size distribution.
    - Thirdly, the model and the video analysis via NTA should be run with a finer bin mesh to reduce the impact of smoothing due to the weighting of the model.
    - Lastly, investigations should examine differences between LSSE analysis performed on the concentration and LSSE data performed on the particle size distribution function.
- It is urged that investigations be made analyzing the effect that size of time step and numerical scheme have on the output of the model, to determine if substituting the

numerical scheme with a method that has a larger region of absolute stability in the negative half-plane is necessary for improved accuracy.

6. References

[1] Xing, B., Vecitis, Chad D., & Senesi, N. (2016). *Engineered nanoparticles and the environment : Biophysicochemical processes and toxicity* (Wiley-IUPAC series on biophysico-chemical processes in environmental systems). Hoboken, New Jersey: John Wiley & Sons.

[2] Basavegowda, N., Mishra, K., & Lee, Y. (2017). Synthesis, characterization, and catalytic applications of hematite (α -Fe 2 O 3) nanoparticles as reusable nanocatalyst. *Advances in Natural Sciences: Nanoscience and Nanotechnology, 8*(2), 6.

[3] Nason, J. (2006). *Particle aspects of precipitative softening: Experimental measurement and mathematical modeling of simultaneous precipitation and flocculation.* (Vol. 68).

[4] Klaine, S., Alvarez, P., Batley, G., Fernandes, T., Handy, R., Lyon, D., . . . Lead, J. (2008). Nanomaterials in the environment: Behavior, fate, bioavailability, and effects. *Environmental Toxicology and Chemistry, 27*(9), 1825-1851.

[5] Piccinno, F., Gottschalk, F., Seeger, S., & Nowack, B. (2012). Industrial production quantities and uses of ten engineered nanomaterials in Europe and the world. *Journal of Nanoparticle Research, 14*(9), 1-11.

[6] Maurer-Jones, M., Gunsolus, I., Murphy, C., & Haynes, C. (2013). Toxicity of Engineered Nanoparticles in the Environment. *Analytical Chemistry,85*(6), 3036-3049.

[7] Benjamin, M., & Lawler, Desmond F. (2013). *Water quality engineering: Physical/chemical treatment processes*. Hoboken, New Jersey: Wiley.

[8] Han, M., & Lawler, D. (1992). The (Relative) Insignificance of G in Flocculation. *Journal - American Water Works Association, 84*(10), 79-91.

[9] Stankus, D. (2011). *Interactions between natural organic matter and gold nanoparticles stabilized with different organic capping agents*. Oregon State University.

[10] Nowicki, Waldemar, & Nowicka, Grazyna. (1994). Verification of the Schulze-Hardy rule: A colloid chemistry experiment. *Journal of Chemical Education, 71*(7), 624.

[11] Smith, B., Pike, D., Kelly, M., & Nason, J. (2015). Quantification of Heteroaggregation between Citrate-Stabilized Gold Nanoparticles and Hematite Colloids. *Environmental Science & Technology, 49*(21), 12789-97.

[12] Weber, C., Environmental Monitoring Systems Laboratory, & United States. Environmental Protection Agency. (1993). *Methods for measuring the acute toxicity of effluents and receiving waters to freshwater and marine organisms* (4th ed.). Cincinnati, Ohio: Environmental Monitoring Systems Laboratory, Office of Research and Development, U.S. Environmental Protection Agency.

[13] Pike, D. (2014). *Heteroaggregation of gold nanoparticles with model colloids and the influence of environmental aqueous chemistry*. Corvallis, Or.: Oregon State University.

[14] Chen, K., Mylon, S., & Elimelech, M. (2006). Aggregation kinetics of alginate-coated hematite nanoparticles in monovalent and divalent electrolytes. *Environmental Science & Technology, 40*(5), 1516-1523.

[15] Nason, J., Mcdowell, S., & Callahan, T. (2012). Effects of natural organic matter type and concentration on the aggregation of citrate-stabilized gold nanoparticles. *Journal of Environmental Monitoring, 14*(7), 1885-1892.

[16] Chen, K., Smith, B., Ball, W., & Fairbrother, D. (2010). Assessing the colloidal properties of engineered nanoparticles in water: Case studies from fullerene C-60 nanoparticles and carbon nanotubes. *Environmental Chemistry, 7*(1), 10-27.

[17] U.S. Geological Survey, 2016, National Water Information System data available on the World Wide Web (USGS Water Data for the Nation), accessed April 10, 2018, at URL [https://nwis.waterdata.usgs.gov/or/nwis/uv?cb_00095=on&format=gif_default&site_no=14211720&period=&begin_date=2014-07-01&end_date=2014-07-31].

[18] Baalousha, M., Manciulea, A., Cumberland, S., Kendall, K., & Lead, J. (2008). Aggregation and surface properties of iron oxide nanoparticles: Influence of ph and natural organic matter. *Environmental Toxicology and Chemistry, 27*(9), 1875-1882.

[19] Holthoff, Egelhaaf, Borkovec, Schurtenberger, & Sticher. (1996). Coagulation rate measurements of colloidal particles by simultaneous static and dynamic light scattering. *Langmuir, 12*(23), 5541-5549.

[20] Mehrabi, K., Nowack, B., Arroyo Rojas Dasilva, Y., & Mitrano, D. (2017). Improvements in Nanoparticle Tracking Analysis To Measure Particle Aggregation and Mass Distribution: A Case Study on Engineered Nanomaterial Stability in Incineration Landfill Leachates. *Environmental Science & Technology, 51*(10), 5611-5621.

[21] Amal, Raper, & Waite. (1990). Fractal structure of hematite aggregates. *Journal of Colloid And Interface Science, 140*(1), 158-168.

[22] LeVeque, R. (2007). *Finite difference methods for ordinary and partial differential equations : Steady-state and time-dependent problems*. Philadelphia, PA: Society for Industrial and Applied Mathematics.

Appendices

Appendix A1. Initial Rates of Aggregation for Hematite in KCl

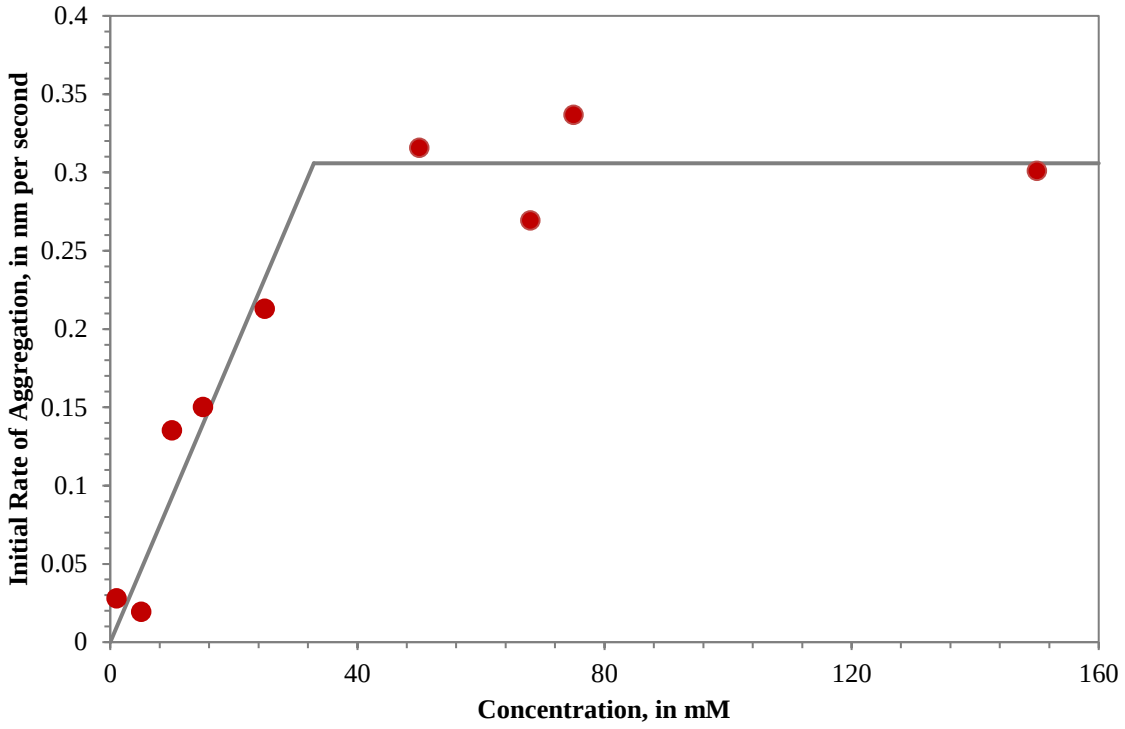

Figure 16. Initial rates of aggregation calculated using the time elapsed between the initial measurement and when the hydrodynamic diameter reached 1.3($D_{h,0}$). The horizontal line represents the average initial rate of aggregation for the trials from 0.050 M to 0.150 M KCl.

Appendix A2. KCl and $CaCl_2$ CCC data for 10 mg L^{-1} Hematite

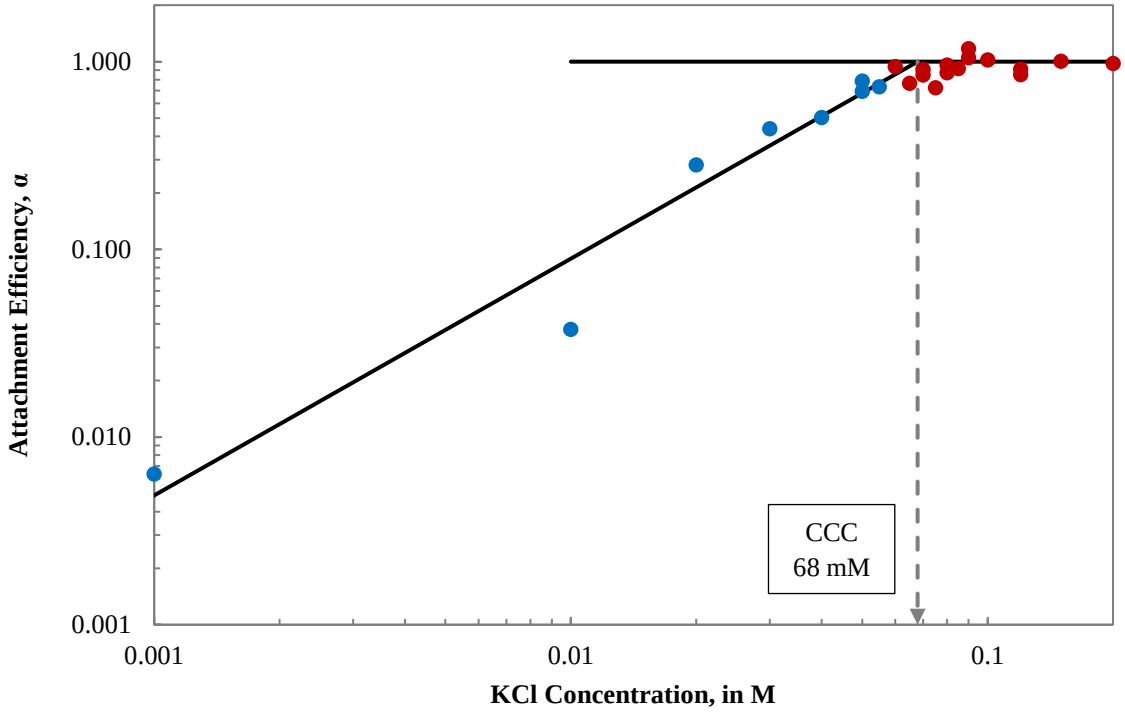

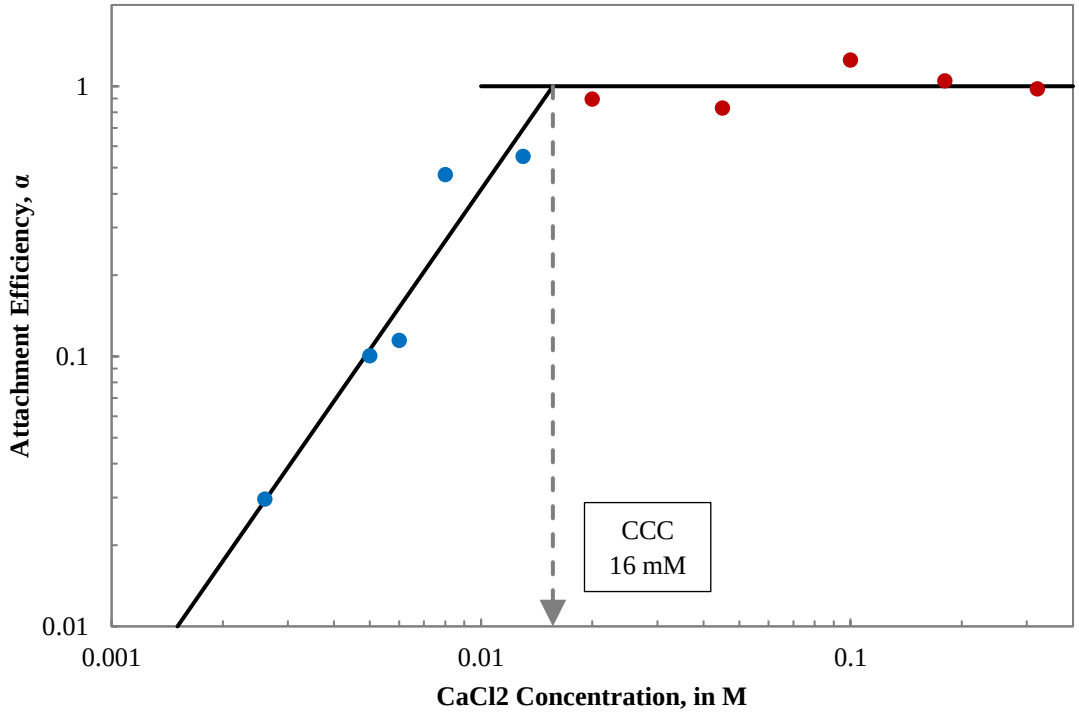

Appendix A3. Summary of Model Inputs

Number of particle sizes: 100

Number of z boxes: 1

Number of x components: 1

Number of timesteps: 1

Minimum time step: 0.05 second

Maximum time step: 1 second

$LogV_1$: -9.281 (V in μm^3)

$LogV_{step}$: 0.09 (V in μm^3)

Density, ρ: 5.26 g/cm^3

Temperature: 298 K

Initial time: 0 s

Maximum time: 1800 s

Viscosity: 0.01002 g/cm•s

Velocity Gradient, G: 0 s^{-1}

Attachment Efficiency, α_{emp}: varied

Tau: 0

Relative Error: 0.001

Brownian motion switch: 2 (curvilinear model)

Fluid shear switch: 0 (not considered)

Differential sedimentation switch: 0 (not considered)